Economic Geology
Vol. 90, 1995, pp. 860–876

Mesothermal-Type Mineralization in the Sabie-Pilgrim's Rest Gold Field, South Africa

R. H. BOER,

Economic Geology Research Unit, University of the Witwatersrand, Johannesburg 2050, South Africa

F. M. MEYER, L. J. ROBB,

Department of Geology, University of the Witwatersrand, Johannesburg 2050, South Africa

J. R. GRANEY, T. W. VENNEMANN, AND S.E. KESLER

Department of Geological Sciences, University of Michigan, Ann Arbor, Michigan 48019

Abstract

We describe here a different class of mesothermal gold deposit at Sabie-Pilgrim's Rest which is probably associated with the Bushveld igneous event in South Africa. Pressure and temperature estimates indicate that the ore fluids of the Sabie-Pilgrim's Rest gold field, which occurs within the Early Proterozoic Transvaal Supergroup, were similar to those of mesothermal gold deposits. However, a number of features distinguish the Sabie-Pilgrim's Rest ores from typical mesothermal deposits: (1) the presence of ubiquitous Cu and Bi in addition to Au, Ag, As, and Sb; (2) high salinities (mean ≈12 wt % NaCl equiv); (3) low mean bulk CO_2 content (≈5 mole %); (4) veins largely hosted within a platform carbonate sequence; and (5) mineralization along both vertical and horizontal (stratiform) veins, showing a clear genetic link. Characteristic features of the Sabie-Pilgrim's Rest gold field that correspond to those within the above spectrum of mesothermal gold deposits include: (1) comparable light stable isotope (δD, $\delta^{18}O$, $\delta^{34}S$) ranges, together with a lack of isotopic evidence for meteoric water involvement; (2) high Au/Ag ratios; (3) presence of ore shoot structures, which are highly characteristic of mesothermal gold deposits; (4) variably deformed structures within individual sheeted veins which point toward cyclic opening and quartz accretion events separated by episodes of deformation; and (5) fluid inclusion properties which indicate high fluid pressures during entrapment.

Bushveld magmatism is thought to have been the main heat source responsible for generating the hydrothermal cell that resulted in the formation of the Sabie-Pilgrim's Rest gold field. Mineralization involved an originally pristine fluid transporting metals that were probably derived from the same source, as well as a measure of connate waters from the granitic basement and the overlying sedimentary rocks. The fluid was relatively acidic and anoxic and equally efficient in transporting gold either as a bisulfide complex or a chloride complex. Gold precipitation took place as a result of (1) a decrease in sulfur activity within the ore-bearing fluid because of sulfide precipitation, and (2) changes in the fluid chemistry as a result of fluid immiscibility.

Introduction

VEIN systems that formed under mesothermal conditions have been important sources of gold for over a century (Lindgren, 1933). Most mesothermal deposits are found in metamorphic terranes, sometimes near deep felsic intrusions, and include the important greenstone gold deposits of the Archean (e.g., Robert and Kelly, 1987). The Sabie-Pilgrim's Rest district in the eastern Transvaal (Fig. 1) consists of numerous mines, of which four produced more than 1 Moz, and covers an area of 600 km^2 (Reinecke and Stein, 1930; Swiegers, 1949). A total of 168 metric tons of gold has been produced from this goldfield since 1872. Although the Sabie-Pilgrim's Rest gold field has been overshadowed by the Barberton and Witwatersrand gold mining districts, it remains the third largest gold producer in South Africa and would be considered a large district in most other parts of the world. For instance, in terms of total gold production it is comparable with the Juneau gold belt in Alaska (Redman, 1986).

The Sabie-Pilgrim's Rest gold field is found near the eastern margin of the Bushveld Complex (Fig. 1). It is thought that the complex covered the gold field during the time of mineralization and that folding and multiple periods of erosion have reduced the extent of the complex and enclosing strata (Cheney and Twist, 1991). Furthermore, the gold field is intersected by one of the two concentric structures along which feeder sites to the Bushveld Complex (such as Losberg and Uitkomst) are arranged (Sharpe et al., 1981). This setting suggests that a genetic link exists between the Sabie-Pilgrim's Rest gold field and the Bushveld igneous event. Layered basic igneous complexes are not commonly thought to be associated with hydrothermal gold deposits. Thus, the Sabie-Pilgrim's Rest gold field could provide insights into the source of fluids in mesothermal gold deposits, as well as the nature of hydrothermal systems around large mafic intrusions. In view of the widespread nature of such mafic complexes, any such association would be significant for gold exploration.

Geologic Relations

Geologic setting

In the Sabie-Pilgrim's Rest area (Fig. 1), the protobasinal Wolkberg Group forms the lowermost part of the Early Proterozoic Transvaal Supergroup and lies unconformably on the Archean Nelspruit batholith. The latter comprises a large, composite body of granodiorite-adamellite (Robb et al., 1983) which contains local small pegmatites but is otherwise barren of mineralization. Disconformably overlying the Wolkberg

0361-0128/95/1707/860-17$4.00

DOI: 10.2113/gsecongeo.90.4.860

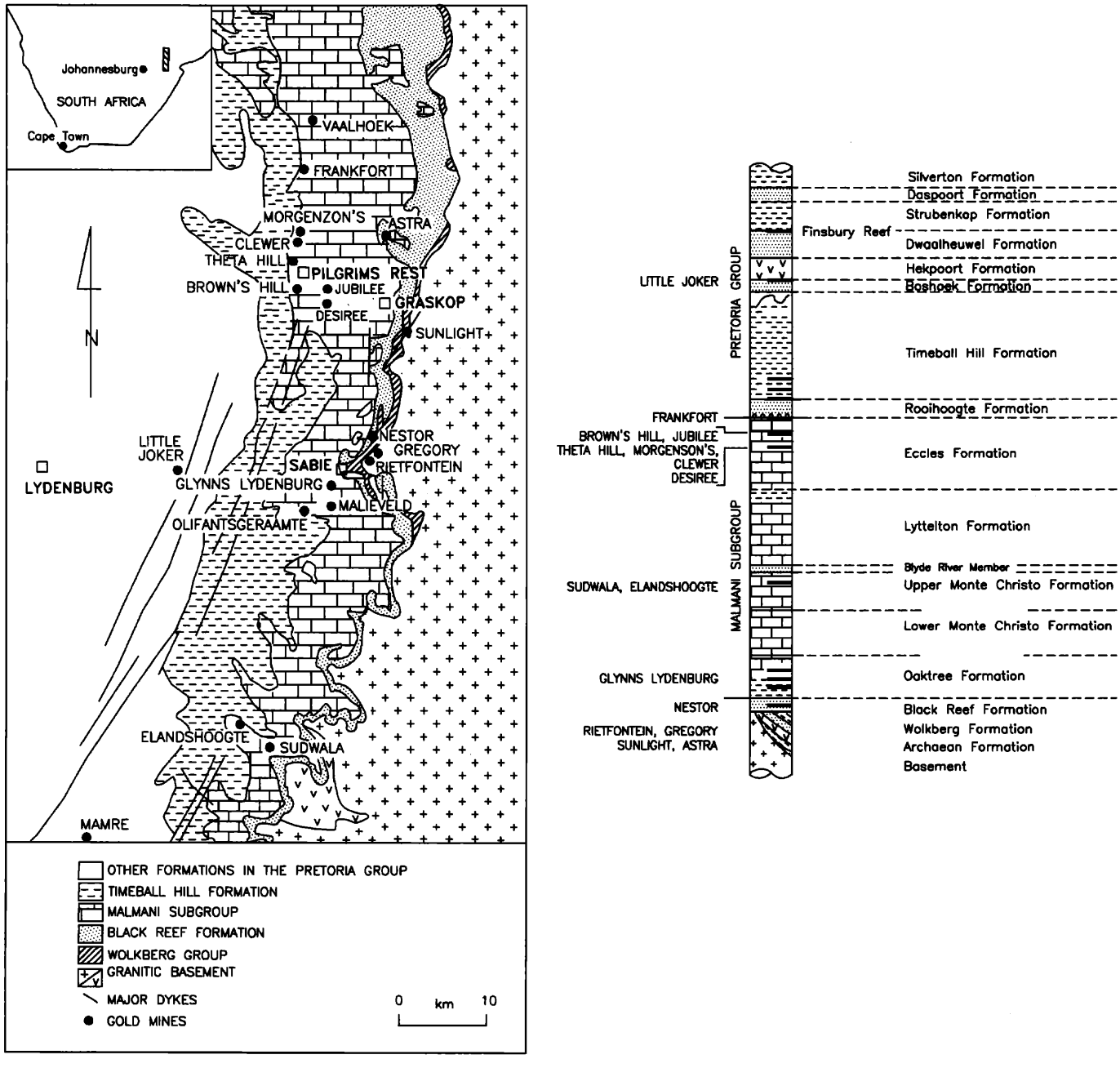

FIG. 1. Geologic map of the Sabie-Pilgrim's Rest gold field with schematic stratigraphic column (not to scale). Positions of mines are indicated (modified after Harley and Charlesworth, 1995).

Group are siliciclastic sedimentary rocks of the Black Reef Formation, which forms the top of the main escarpment in the area. The Black Reef Formation consists of feldspathic quartzite with interlayered lenses of grit and conglomerate. The platform carbonates of the Malmani Subgroup (part of the Chuniespoort Group) conformably overlie the Black Reef Formation. The Malmani Subgroup consists of the Oaktree, Monte Christo, Lyttelton, and Eccles Formations and is host to the majority of gold-bearing quartz veins. Formational divisions within the Malmani Subgroup are based mainly on the variations in chert content and type of algal structures found in the dolomite (Button, 1973; Clendenin, 1989). Successive regressive and transgressive sedimentary cycles have been recognized in the Malmani Subgroup (Clendenin, 1989; Tyler, 1989). The Oaktree Formation is comprised of iron- and manganese-rich dolomite, carbonaceous shale, and quartzite, whereas the Monte Christo Formation is characterized by oolitic carbonate rocks (Button, 1986). Siliciclastic sediments (quartzite and/or shale) mark the base of the overlying chert-poor Lyttelton Formation, which is composed of dark-colored quartz arenite in the Sabie-Pilgrim's Rest area (Tyler, 1989). This unit grades upward to the upper dolomite and chert zone of the Eccles Formation. Following the deposition of these sediments, the strata were exposed and an

extensive erosional period ensued. This resulted in the formation of a widely developed chert breccia and chert pebble conglomerate, the so-called Bevetts Conglomerate, at the base of the siliciclastic-dominated Pretoria Group. The Pretoria Group consists of alternating shale and quartz arenites, with minor conglomerates, granulestones, and interlayered volcanic units (Button, 1973). This succession, as developed in the eastern Transvaal, is approximately 7,000 to 8,000 m in thickness (Button, 1973, 1986).

A large number of basic dikes and sills, of different ages, have intruded into the Transvaal Supergroup in the Sabie-Pilgrim's Rest area, and increase in frequency upward in the stratigraphy (Sharpe, 1984; Tyler, 1989). Sharpe (1981) and Willemse (1959) distinguished between pre-Bushveld diabase dikes-sills, and syn-Bushveld dikes-sills of pyroxenitic composition. The pre-Bushveld diabase intrusions are intersected by gold-mineralized quartz veins (e.g., Olifantsgeraamte mine), whereas the pyroxenitic syn-Bushveld dikes-sills crosscut mineralization (e.g., Frankfort mine). The pre-Bushveld dikes-sills were metamorphosed to greenschist facies prior to emplacement of the mafic phase of the Bushveld Complex (Sharpe, 1981). The Transvaal sedimentary and volcanic rocks are locally metamorphosed by these intrusions (Button, 1986). Crosscutting field relations between auriferous quartz veining with pre-Bushveld and syn-Bushveld diabase dikes (Sharpe et al., 1981) yield the only dependable, albeit broad, age constraint. The pre-Bushveld diabase dikes-sills (Willemse, 1959; Sharpe, 1981) are intersected by gold-mineralized quartz veins (e.g., Olifantsgeraamte mine), whereas the pyroxenitic syn-Bushveld dikes-sills crosscut these mineralized quartz veins (e.g., Frankfort mine). These field relations confine the age of mineralization to the early stages of emplacement of the Bushveld Complex, probably postdating emplacement of the mafic phase. The granitic phase of the Bushveld Complex has been dated at 2054.4 ± 1.8 Ma, using the single zircon Pb-evaporation technique (Walraven and Hattingh, 1993).

A prominent series of northeasterly trending lineaments is evident within the gold field. Mafic dike emplacement, postmineralization normal faulting, and limited graben development have occurred parallel to this trend. Field relations (at Gregory and Rietfontein mines) show that the vertical veins divert along lithological contacts into a horizontal orientation, suggesting a genetic correlation between the vertical and horizontal veins. Similar indications of a possible link between the vertical and horizontal veins can also be found at the Pigeon vein (P.N. Bentley, pers. commun., 1993) and the Astra mine (Anderson, 1992). Bedding in the goldfield dips between 4° and 15° to the west. Vein emplacement is controlled by low angle ($\sigma_1 \leq 5°$), southeastward-verging bedding-parallel simple shear thrusts (Harley and Charlesworth, 1992). Small-scale duplexes and shallowly westward-dipping ramp structures, as well as asymmetric folds, are typically developed within the mineralized carbonaceous shale. Within these shales, a well-developed subhorizontal planar fabric, comprising a closely spaced cleavage, is developed. Cleavage surfaces often bear slickensides which indicate early faulting. Fine-grained euhedral pyrite occurs as fabric-parallel layers within the shales (Harley and Charlesworth, 1992), whereas mineralogically, they are composed of sericite with minor amounts of quartz and organic carbon.

Wall-rock alteration associated with the quartz veins within the sediments is restricted to meter-wide zones of silicification, whereas alteration within dike-sill-hosted mineralization comprises quartz-sericite-carbonate-pyrite.

Mineralogy and Geochemistry

Nature and mineralogy of veins

Sabie-Pilgrim's Rest-type mineralization is epigenetic and confined to transgressive, vertical veins[1], strata-bound horizontal veins, and sill-dike-associated veins. The horizontal veins are composed of multiple sheets of quartz-carbonate (dolomite, ferro-dolomite, calcite), usually associated with thin slivers of carbonaceous shale and dolomite host rock (Fig. 2A and B). Anhedral quartz, similar to that described by Dowling and Morrison (1989), comprises the bulk of the veins. Small vugs lined with euhedral crystals of quartz are found locally (Fig. 2C). The average thickness of the horizontal veins ranges from 5 to 40 cm. Massive quartz stockworks and breccias, consisting of a mixture of vein material and silicified host-rock fragments, are locally abundant and economically significant (Fig. 2D). Surrounding such zones of vein thickening (commonly up to 3 m) are subparallel stringer veins, which are mineralized locally, and occasional subvertical stringer veins. These stringers pinch out within tens of centimeters from the main vein component. The gold grade is highly variable (from traces to over 60 g/ton; Fowler, 1968), with the overall districtwide grade being on the order of 9 g/ton Au. In most deposits there are gradational differences in gold grade along strike such that alternations between ore-grade zones and low-grade waste zones can be distinguished. This situation gives rise to a characteristic ore shoot pattern (Wybergh, 1925; Zietsman, 1967), with little evidence of mineralogical or elemental zoning on a deposit scale. Furthermore, no consistent zonation patterns in terms of the sulfide mineralogy are obvious on a regional scale within the gold field. The horizontal veins associated with the Oaktree Formation and the upper Lyttleton and Eccles Formations, as well as the vertical veins (Boxall, 1938), are characterized by a more complex suite of ore minerals (i.e., pyrite, arsenopyrite, fahlores, chalcopyrite, bismuth sulfosalts, and bismuth), whereas the horizontal veins occurring at intermediate stratigraphic positions in the Monte Christo and lower Lyttleton Formations contain predominantly pyrite and lesser amounts of chalcopyrite and sphalerite.

Three stages of sulfide mineralization have been identified (Meyer et al., 1986):

Stage 1. Early diagenetic pyrite from the wall rock is found associated with the gold-mineralized veins. The pyrite is euhedral to subhedral and virtually free from inclusions of other minerals, apart from a few gold grains.

Stage 2. This stage is coarser grained pyrite containing inclusions of chalcopyrite and gold, along with slightly later arsenopyrite that also contains inclusions of chalcopyrite and

[1] Within the Sabie-Pilgrim's Rest gold field, individual orebodies or quartz-carbonate-sulfide-gold veins are locally referred to as "reefs."

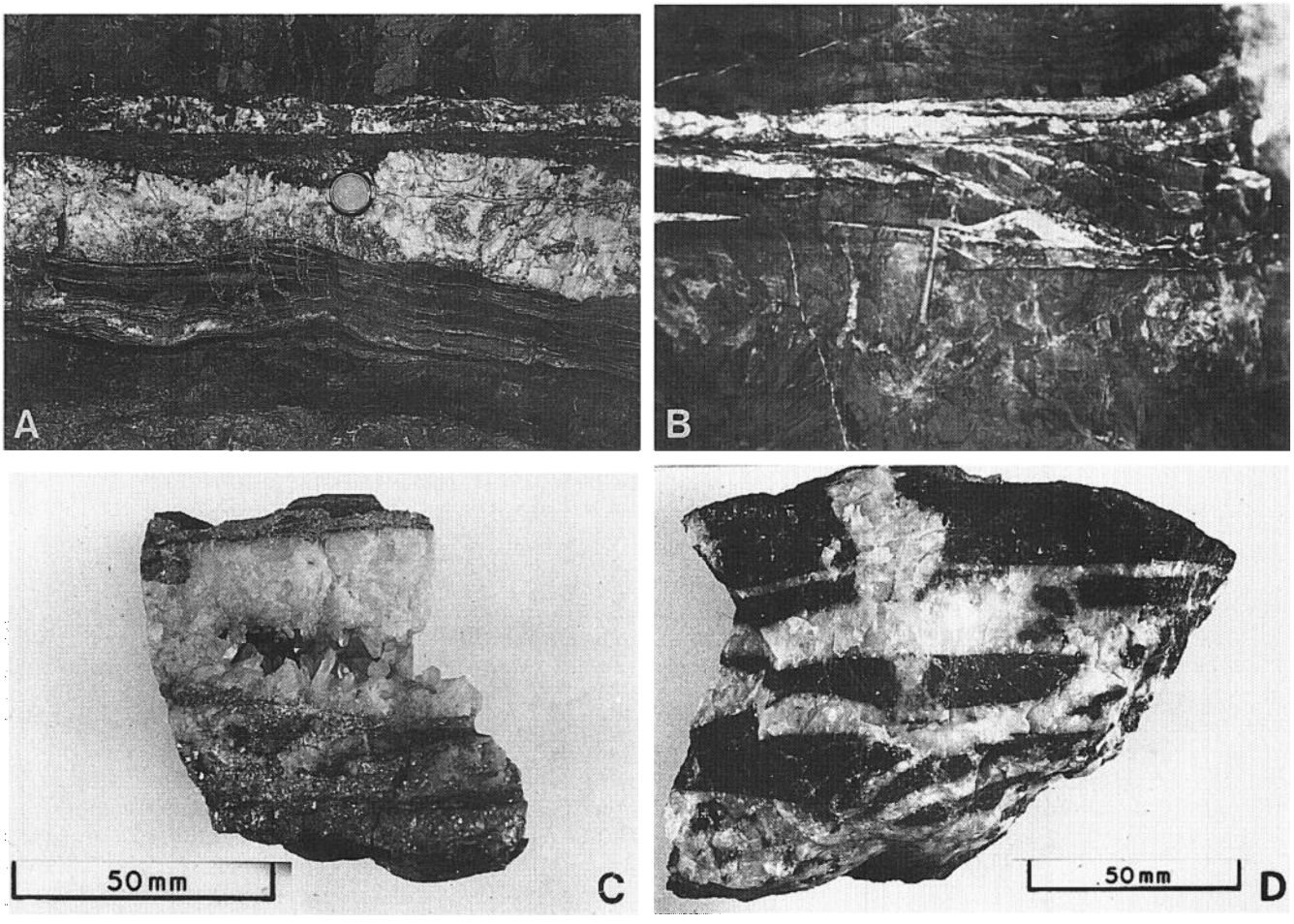

FIG. 2. Underground exposure of gold-bearing veins. A. Typical quartz carbonate vein with abundant coarse-grained pyrite, Elandshoogte mine. B. Sheeted appearance (ribbon texture) of vein with graphitic and dolomitic wall-rock inclusions, Glynns-Lydenburg mine, Sheba section. C. Comb quartz, Clewer mine. D. Quartz-cemented breccias, Elandshoogte mine. Photographs A and D courtesy of Michael Harley.

tetrahedrite and that, in places, overgrows and replaces pyrite. This mineralization episode was also accompanied by quartz and carbonate.

Stage 3. After a period of brittle deformation of the orebodies, as indicated by abundant fractures in pyrite and arsenopyrite and also by clasts of wall-rock material within quartz, a later suite of fahlores, chalcopyrite, bismuth sulfosalts, native bismuth, and gold was deposited.

There is a distinct increase in gold content toward the later stages of sulfide mineralization, with most of the gold being emplaced at a very late stage. Gold associated with each of the three stages of sulfide mineralization has a characteristic fineness that decreases with an increasing complexity of the sulfide paragenesis (avg fineness values: stage 1 = 952, stage 2 = 889, stage 3 = 871, avg fineness for the Sabie-Pilgrim's Rest gold field = 893). The paragenetic sequence in sill-dike-associated deposits (i.e., Olifantsgeraamte and Vaalhoek mines) appears to be less complex, with only one generation of pyrite and chalcopyrite developed, which contains round inclusions of gold. Gangue minerals in the veins are dominated by quartz, with lesser ferruginous carbonates and local muscovite, scheelite, and rare rutile.

Fluid inclusion petrography

Fluid inclusion data were obtained by microthermometric heating and freezing, using the standard techniques described by Roedder (1984, p. 196–201). Temperatures of phase changes were obtained on a Fluid Inc.-adapted U.S.G.S. heating-freezing system, with the thermocouple calibrated against synthetic fluid inclusions (Sterner and Bodnar, 1984). Microthermometric measurements were made on inclusions that could be confidently classified and were large enough to permit easy observation of phase changes (i.e., $>5\mu m$). Salinities were related to freezing point depression using the equation of Bodnar (1993).

All of the quartz veins examined experienced repeated fracturing in the presence of aqueous fluids as shown by abundant planes of secondary inclusions observed at low magnification. The high density of randomly oriented fractures decorated with fluid inclusions made it difficult to determine whether a given inclusion was fracture related or was trapped during crystal growth. For this reason, the authors have not attempted to classify fluid inclusion types according to the criteria of Roedder (1984, p. 13–26) but have rather related groups of inclusions to various stages of vein filling. Two

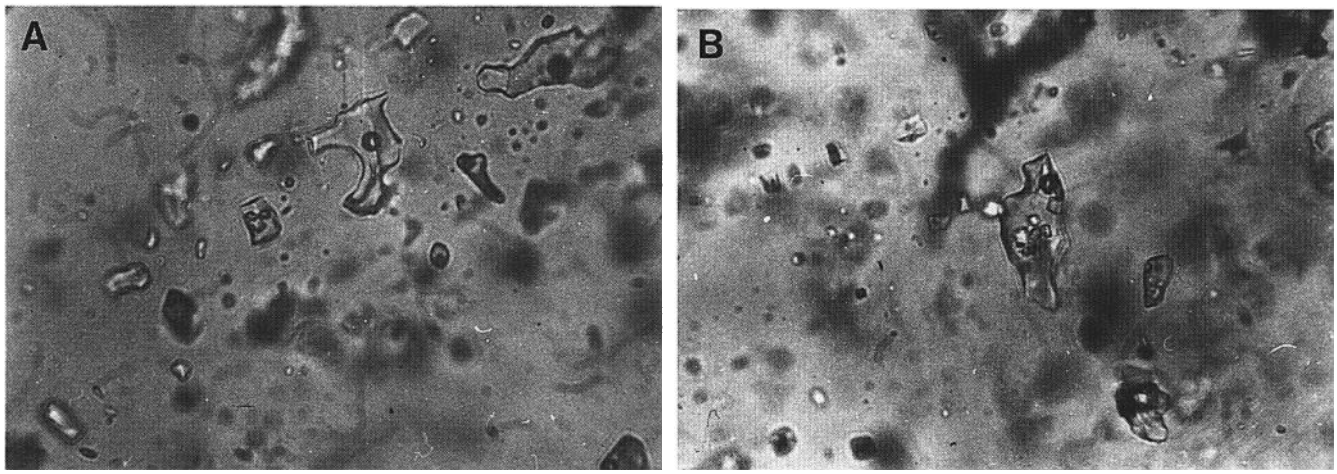

FIG. 3. A. Type 1 fluid inclusions in quartz at room temperature. These are filled with an aqueous liquid and a carbonic phase. B. Type 2 inclusions typified by multiple daughter crystals. Late-stage type 3 aqueous inclusions occur with or without vapor bubbles. See text for detailed discussion.

optically distinct varieties of quartz were observed, an early, gray to milky translucent variety, and a later transparent type which either engulfs or occurs along microfractures in the milky quartz and is characterized by a distinctly different fluid inclusion population. The clear quartz is not associated with gold. In all of the samples studied from the horizontal veins, approximately 95 percent of the quartz is of the early, milky variety. Quartz from the Sabie-Pilgrim's Rest gold field generally contains a number of apparently coexisting fluid inclusion populations within a single field of view.

Type 1 inclusions: High CO_2: This is the dominant fluid inclusion type and exhibits three phases, an aqueous liquid, a carbonic liquid, and a vapor bubble, at room temperature (Fig. 3A), with occasional daughter crystals. The liquid to vapor ratio, as well as H_2O/CO_2 ratios, varies to such an extent that the type 1 inclusions were subdivided into three categories: (i) aqueous inclusions containing an aqueous liquid, a small carbonic vapor bubble, and occasionally a single cubic daughter crystal; (ii) large single-phase liquid carbonic inclusions with vapor bubbles that appear during cooling; and (iii) a spectrum of three-phase inclusions with variable H_2O/CO_2 ratios, seldom containing a daughter crystal. Contemporaneity of fracture-related aqueous and carbonic fluid inclusions was confirmed by cathodoluminescence studies, which show that the type 1 inclusions occur together within individual quartz domains. Furthermore, aqueous and carbonic inclusions occasionally occur along the same healed fracture. The continuum in H_2O/CO_2 ratios shown by these fluids also strongly suggests a close genetic relation between the two fluids. The morphology of this inclusion type varies from irregular to rounded, with some equidimensional negative crystal shapes. The size of the inclusions ranges from 5 to 30 μm.

Final melting temperatures (T_m) of the aqueous phase range from −21.2° to −4.3°C, corresponding to a salinity range of 23.5 to 5.5 wt percent NaCl equiv. The majority of inclusions containing carbonic species decrepitate between 170° and 290°C, prior to bulk homogenization (T_h), suggesting high internal fluid pressures. However, T_h measurements that were obtained range from 105° to 255°C, corresponding to high bulk densities of 0.857 to 1.053 g/cm^3. Comparison of homogenization and final melting temperatures for the various veins show different salinities for the three veins and confirm the salinity ranges within individual veins (Fig. 4). First melting temperatures for the carbonic phase are slightly below the value for pure CO_2 and confirm the presence of other gaseous species, such as CH_4 and N_2. Two populations of carbonic inclusions were recognized on the basis of the CO_2 homogenization temperatures, with histogram peaks occurring at 10° and 23°C, respectively (Fig. 5). The different densities, indicated by these different temperatures, suggest that two generations of carbonic fluid influx occurred.

Type 2 inclusions: Low CO_2 + high salinity: This type of inclusion is characterized by an aqueous liquid, a vapor bubble, and at least one daughter crystal at room temperature (Fig. 3B). Low initial ice-melting temperatures, plus the presence of another daughter crystal in addition to halite (or

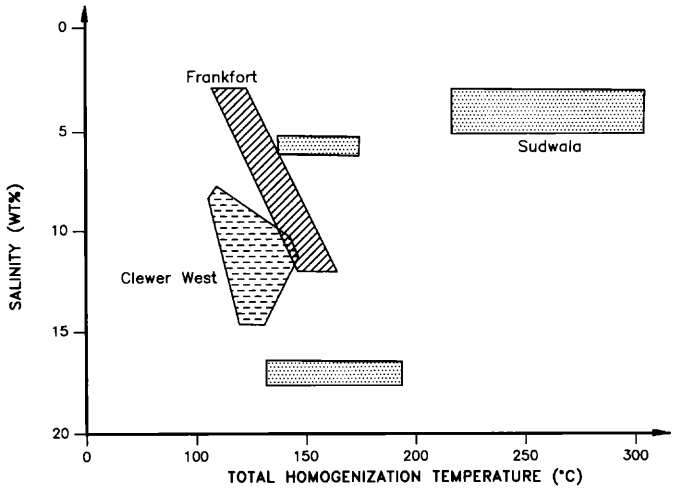

FIG. 4. Homogenization temperature versus salinity for type 1 inclusions. The boxes identify the domains of the mineralizing fluids of different deposits.

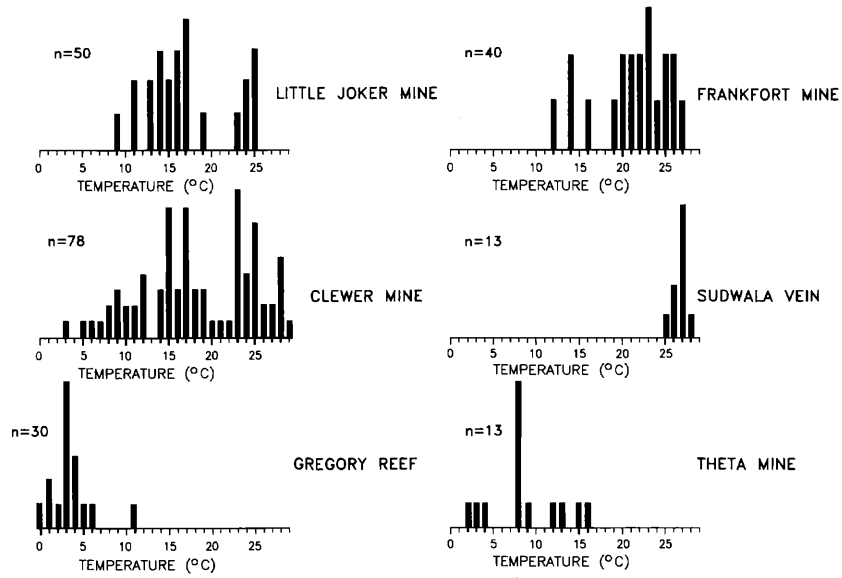

FIG. 5. Histograms depicting homogenization temperatures of the carbonic phase in type 1 fluid inclusions.

sylvite) indicate that calcium or magnesium chlorides are probably present in the liquid. Carbonic species are frequently present but are not visible and are only evident in the formation of clathrates that obscure accurate determination of final melting temperatures. This type of inclusion is common in the vertical veins, but does not occur in the stratabound horizontal veins. Homogenization temperatures of gases into the liquid phase in these inclusions range from 105° to 165°C, whereas dissolution temperatures for the daughter phases (total homogenization) plot in the range 220° to 245°C, corresponding to salinities of around 33 wt percent NaCl equiv. It is very common for type 2 fluid inclusions to decrepitate before total homogenization occurs.

Type 3 inclusions: Low CO_2 + low salinity: These inclusions contain an aqueous liquid, with or without a vapor bubble at room temperature, and are believed to be the last-formed inclusion type. They are found in both the milky and clear quartz varieties. However, in the volumetrically minor late-stage clear quartz these inclusions predominate, whereas carbonic and aqueous saline inclusions are rare. Crosscutting relations between type 3 and 1 inclusions prove that the former postdate the carbonic-rich inclusions. Final melting temperatures center around −4.5°C (corresponding to a salinity of about 7 wt percent NaCl equiv), and homogenization temperatures range from 110° to 135°C (density range: 1.00–0.98 g/cm^3). The absence of vapor bubbles in many of these late fluid inclusions suggests low entrapment temperatures and confirms the late temporal relations.

Quadrupole mass spectrometer gas analyses: Quadrupole mass spectrometer gas analyses were performed on pieces of fluid inclusion wafers (less than 2 mm in diam) with a total mass of less than 50 mg. Gases were released from quartz wafers by crushing the samples at 110°C under vacuum in a modified Nupro® valve, from which they were passed directly into a VG SXP600 quadrupole mass spectrometer via a short conduit designed to maximize conductance and minimize adsorption between sample and ionizing filament (Table 1). Data for 16 specified masses were collected in a cycling period of about 0.2 s, which permitted simultaneous determination of H_2O, CO_2, CH_4, C_2H_6, N_2, Ar, H_2S, SO_2, HCl, and H_2. Selection of the specified masses was based on an evaluation of the integrated mass response in terms of the composition of the common constituents found in fluid inclusions. Total response for each mass was obtained by integrating under the individual response-time curve for each mass from the time of crushing until the signal returned to background levels. The integrated response for each mass was converted to mole fractions for the gases of interest using a matrix-inversion procedure that takes into account fragmentation patterns and relative sensitivities (to N_2) determined for the specific instrument utilized (Jones and Kesler, 1992). These values were then normalized and converted to mole percent. Calibration of crush analysis yielded detection limits for a gas concentration of 5 ppm in samples containing at least 0.001 μl of fluid. Inclusion fluids were also released from native gold grains by heating to 900°C under vacuum in a silica glass tube until the inclusions decrepitated (Fig. 6A and B). Gases liberated in this manner passed directly into the quadrupole source and produced episodic signal bursts that probably represent decrepitation of individual inclusions. Gas species from individual gold-hosted inclusions with abundances of less than 0.5 mole percent cannot be reported quantitatively and were therefore omitted (Table 2).

Results from bulk fluid inclusion gas analyses are presented in Table 1. Great care has been taken to ensure the dominance of type 1 fluid inclusions within the pure quartz specimens. This was achieved by microscopic selection of doubly polished quartz chip fragments which were clearly dominated by type 1 fluid inclusions. However, it is inevitable that this type of bulk analysis reflects contamination by other fluid populations (Roedder, 1990) and thus represents partially time-integrated fluid chemistry and may not be absolutely

TABLE 1. Compositions of Quartz-Hosted Inclusion Fluids

Sample no.	H_2O	CO_2	CH_4	C_2H_6	N_2	Ar	H_2S	SO_2	HCl	Total
AST109	96.641	3.216	0.078	0.000	0.0000	0.0065	0.0043	0.0007	0.0520	99.998
BM184A	99.538	0.249	0.053	0.069	0.0000	0.0067	0.0170	0.0091	0.0560	99.998
BM184B	99.744	0.127	0.050	0.008	0.0169	0.0019	0.0074	0.0019	0.0430	100.000
BM7384	98.635	1.088	0.157	0.008	0.0138	0.0009	0.0250	0.0005	0.0720	99.999
CLW016	96.969	2.814	0.128	0.017	0.0235	0.0021	0.0047	0.0020	0.0370	99.998
SUD211	99.010	0.758	0.029	0.047	0.0805	0.0041	0.0045	0.0019	0.0650	99.999
FKM075B	84.634	14.930	0.394	0.007	0.0000	0.0009	0.0089	0.0029	0.0120	99.990
FKM076B	94.374	5.363	0.214	0.105	0.0000	0.0026	0.0043	0.0026	0.0210	99.997
GLS052	94.67	5.210	0.046	0.009	0.0181	0.0040	0.0059	0.0015	0.0310	99.996
GRR300	99.482	0.330	0.079	0.021	0.0251	0.0085	0.0085	0.0025	0.0430	99.999
JBH043	89.518	10.313	0.114	0.011	0.0000	0.0020	0.0051	0.0010	0.0290	99.993
LJM090	93.792	5.951	0.178	0.025	0.0000	0.0000	0.0045	0.0007	0.0330	99.984
MGL204	98.824	0.992	0.043	0.079	0.0000	0.0017	0.0050	0.0031	0.0520	99.999
NSM093	99.340	0.529	0.053	0.019	0.0000	0.0048	0.0031	0.0006	0.0500	100.000
NSM098	88.794	10.534	0.561	0.023	0.0000	0.0077	0.0069	0.0024	0.0620	99.991
OGM078	98.491	1.147	0.081	0.074	0.1067	0.0108	0.0140	0.0027	0.0710	99.998
S1017	97.453	2.380	0.081	0.007	0.0181	0.0039	0.0055	0.0012	0.0480	99.998
SUN003	99.150	0.733	0.031	0.019	0.0000	0.0036	0.0032	0.0002	0.0590	100.000
VLH040A	97.421	2.521	0.025	0.009	0.0000	0.0024	0.0041	0.0022	0.0130	99.998
VLH040B	93.265	6.607	0.021	0.014	0.0481	0.0036	0.0055	0.0017	0.0290	99.995

Determined by Quadrupole Mass Spectrometer Gas Analyses (in mole %)

Locality abbreviations: AST = Astra, CLW = Clewer West, FKM = Frankfort, GLS = Glynns Lydenburg Sheba, GRR = Gregory, JBH = Jubilee, LJM = Little Joker, MGL = Morgenzon, NSM = Nestor, OGM = Olifantsgeraamte, S = Elandsdrift, SUD, = Sudwala, SUN = Sunlight, VLH = Vaalhoek

Exact localities of samples obtained from the British Museum (Natural History) (BM) are unknown

representative. H_2O is by far the dominant volatile component in the Sabie-Pilgrim's Rest fluid inclusions and typically comprises 95 to 99 mole percent of the inclusion fluid. CO_2 comprises most of the remaining volatile component (varying between 0.1–15 mole %), whereas the other gases are generally present in amounts smaller than 1 mole percent. The vertical veins and the horizontal veins from lower down in the stratigraphy contain higher concentrations of Ar and HCl, whereas the upper veins contain larger CO_2 and CH_4 concentrations (Fig. 7A and B; Table 1). High HCl concentrations in vertical veins (Fig. 7A) correlate well with high salinities, as indicated by microthermometric measurements, and are probably a result of the hydrolysis of NaCl at higher temperatures. Furthermore, CH_4/CO_2 ratios for inclusion fluids from horizontal veins are significantly higher compared to vertical veins. This difference indicates that the gas content of the veins clearly reflects the host-rock lithology as a consequence of fluid-rock interaction. The higher abundances of CO_2 and CH_4 in the carbonate-hosted veins suggest a contribution of carbonic species from the dolomitic host rock as a result of interaction with the hydrothermal fluid. A possible source for CH_4 is thermocatalysis of organic matter within the vein-associated shale layers (Welhan, 1988). The dominant fluid population in the Sabie-Pilgrim's Rest gold field exhibits variable CO_2/Ar ratios, and depleted N_2 contents. Comparison with the normalized populations of present-day air and air-saturated water suggests that large-scale fluid interaction with air-saturated meteoric water can be ruled out. Average N_2/Ar ratios center around 4.5 (max = 19.6), they are well below those of air (84) or air-saturated ground water (38). The absence of air contamination from the Sabie-Pilgrim's Rest gas analyses is also indicated by the fact that most analyses plot away from modern-day air composition. The Ar probably resulted from the radiogenic decay of potassium, with subsequent incorporation into fluid inclusions.

Decrepitation analyses of individual primary fluid inclusions hosted within single gold grains (Fig. 8) yielded widely variable CO_2/H_2O ratios (Table 2) for fluid inclusions that decrepitated within a restricted temperature range. Ramboz et al. (1982) emphasized the constraints on homogenization phenomena which enable the recognition of fluid immiscibility: (1) the two immiscible fluids must occur within the same region as the sample; (2) the two types of fluid inclusions must homogenize within the same temperature range because trapping is not an instantaneous and strictly isothermal-isobaric process; and (3) although the internal pressures are different before homogenization, because of variable liquid to vapor ratios, the pressures reach the same value at the homogenization temperature (trapping temperature). Therefore, the decrepitation temperatures should also reflect a restricted temperature range. Such a restricted temperature range for gold-hosted fluid inclusions is, however, influenced by other factors, such as the depth of the fluid inclusions beneath the surface of the gold grain. It is unlikely that more than one generation of fluid could have been trapped in a malleable mineral such as gold, which does not easily allow secondary fractures to form. The fact that a single fluid population displaying variable CO_2/H_2O ratios occurs in the same gold grain, together with a relatively restricted range of decrepitation temperatures, is thought to be a good indication of fluid immiscibility during gold precipitation. The recognition of fluid immiscibility in native gold grains provides a mechanism whereby precipitation of gold could have taken place in the Sabie-Pilgrim's Rest gold field. Fluid immiscibil-

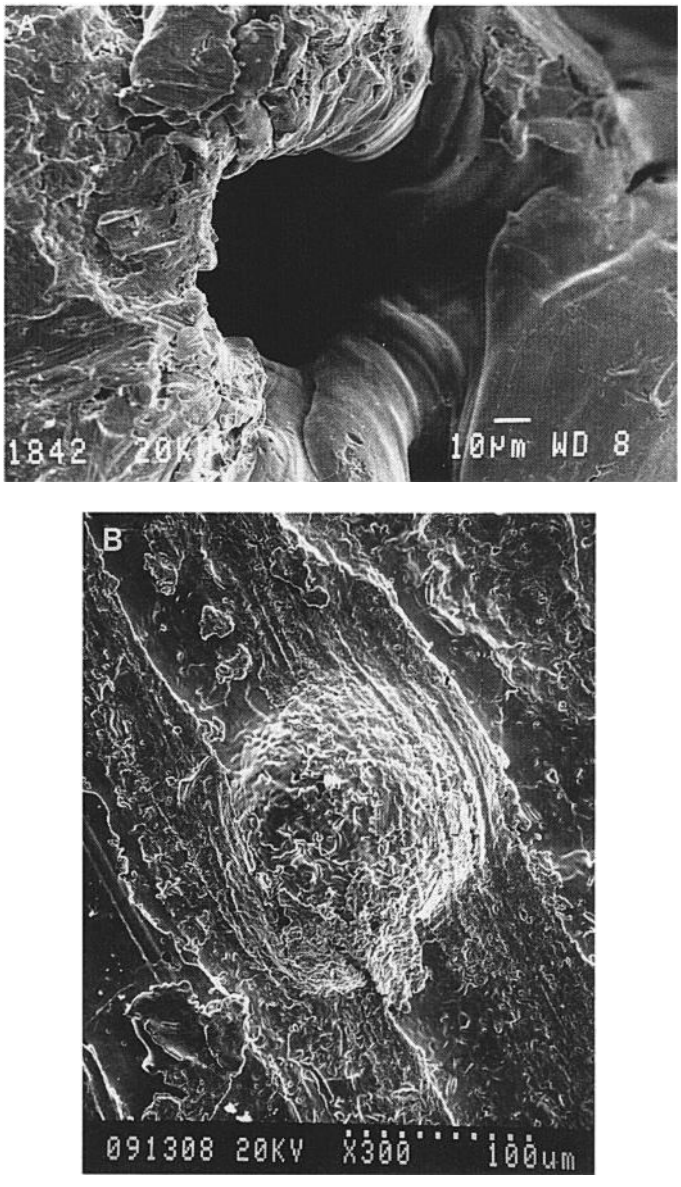

FIG. 6. A. Cavity of a decrepitated fluid inclusion in native gold grain. Diameter of cavity ≈50 µm. B. Striations on cut surface of a native gold grain being distorted as a result of bulging of a near-surface fluid inclusion during a decrepitation run on the quadrupole mass spectrometer.

ity in native metals from a variety of geologic settings, was also reported by Van Hees et al. (1992), using quadrupole mass spectrometer data.

Temporal and genetic interrelations of fluid inclusions: All fluid inclusions observed formed within annealed microfractures. No unambiguous temporal relation could be recognized between type 1 and 2 fluids, but type 3 fluids clearly crosscut type 2 inclusion trails. Type 1 fluids occur in milky quartz in both granite-hosted vertical veins and in sediment- and dike-related horizontal veins, and have also been recognized by Ash and Tyler (1986; types I, II, and IV) and Anderson et al. (1992; types I, II, and III). Type 2 fluids were only observed in vertical veins and correspond to the type III inclusions of Ash and Tyler (1986). Type 3 fluids occur throughout, but form the predominant population in the paragenetically late transparent quartz.

The close association between the three categories of type 1 fluids, and the compositional continuum between these types, suggests that the fluids may be genetically linked. Anderson et al. (1992) also recognized the existence of a compositional continuum in the fluids of the Sabie-Pilgrim's Rest gold field and attributed this to partial mixing between brine and CO_2-rich fluid of discrete origins. Our interpretation of these fluids is that they reflect unmixing of a single CO_2-NaCl-H_2O fluid, since aqueous fluid inclusions, carbonic vapor-rich inclusions, as well as inclusions with variable H_2/CO_2 ratios, are present as the dominant types (type 1 inclusions) in quartz. In addition, the quadrupole mass spectrometer gas data also support immiscibility in the gold-hosted fluid inclusions. Harley and Charlesworth (1995) present evidence for variations in fluid pressure and crack-seal behavior during ore deposition within the Sabie-Pilgrim's Rest gold field. Such a mechanism implies rapid and extreme fluctuations in pressure during ore deposition, which must have affected the position of the H_2O-CO_2 solvus in P-T-X space (Bowers and Helgeson, 1983; Bowers, 1991). Given an original, homogeneous fluid with average mole percent H_2O of 95 to 85 and CO_2 = 5 to 15 mole percent (Table 1) at 320°C and salinity ≈ 12 wt percent NaCl equiv, fluctuations in fluid pressure between assumed values of 2,000 and 1,000 bars would shift the solvus such that the fluid would move from a one-phase into a two-phase field (Fig. 9). The shape of the solvus dictates that unmixing would result in an aqueous component with high, but restricted, salinity and low X_{CO_2} (type 1_i fluid) and a CO_2-rich, low-salinity component (type 1_{ii} fluid). Type 1_{iii} fluid exhibits widely varying H_2O/CO_2 ratios because of the flat-lying geometry of the solvus, a feature which corroborates the compositional continuum observed in type 1 fluids. Bowers and Helgeson (1983) have shown that a high-salinity H_2O

TABLE 2. Quadrupole Mass Spectrometer Gas Analyses of Individual Fluid Inclusions Contained in a Single Pure Gold Grain (in mole %)

H_2O	CO_2	CO_2/H_2O
98.2	1.8	0.018
96.9	3.1	0.032
98.5	1.5	0.015
98.2	1.8	0.018
98.5	1.5	0.015
96.1	3.9	0.041
96.2	3.8	0.040
76.9	23.1	0.300
68.8	31.2	0.453
83.7	16.3	0.195
71.0	29.0	0.408
96.3	3.7	0.038
93.1	6.9	0.074
68.6	31.4	0.458
90.2	9.8	0.109
91.4	8.6	0.094
93.7	6.6	0.071
80.6	19.4	0.241
64.9	35.1	0.541
94.3	5.7	0.060
58.9	41.1	0.698
86.8	13.2	0.152

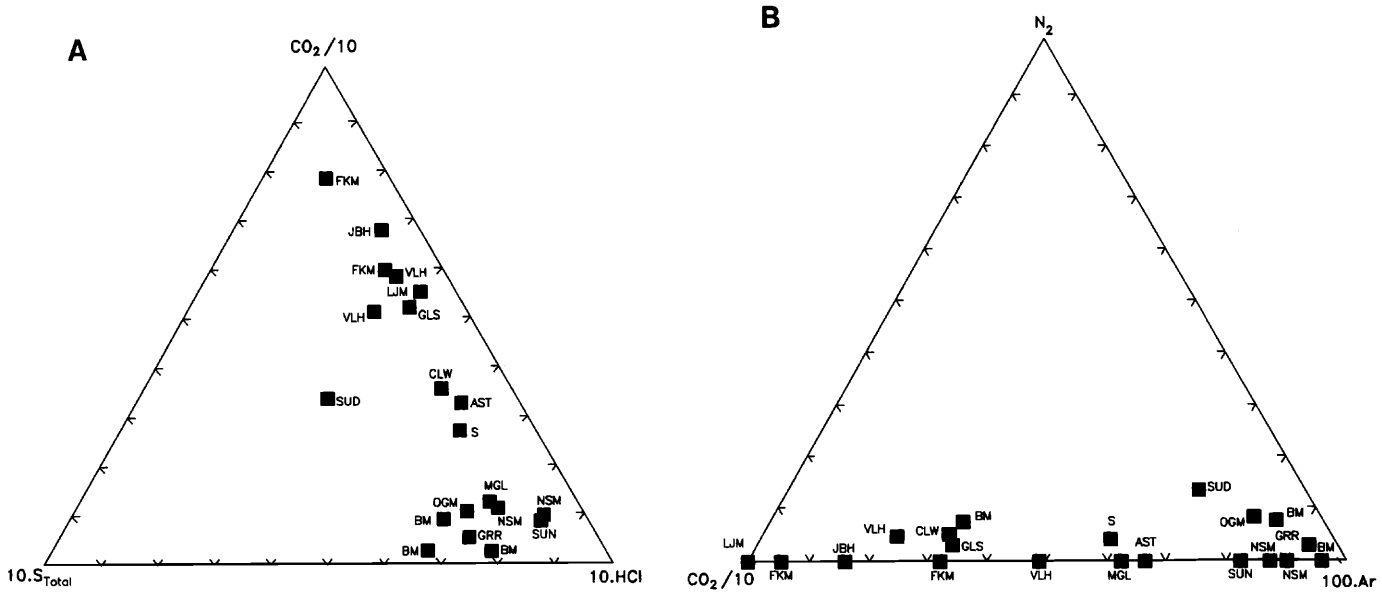

FIG. 7. A. Relative CO_2, S_{total}, and HCl contents of hydrothermal gases from quartz specimens of the Sabie-Pilgrim's Rest gold field. B. Ternary diagram presenting the CO_2, N_2, and Ar contents of inclusion fluids from the Sabie-Pilgrim's Rest gold field. Locality abbreviations: AST = Astra, CLW = Clewer West, FKM = Frankfort, GLS = Glynns Lydenburg Sheba, GRR = Gregory, JBH = Jubilee, LJM = Little Joker, MGL = Morgenzon, NSM = Neston, OGM = Olifantsgeraamte, S = Elandsdrift mine, SUD = Sudwala, SUN = Sunlight, VLH = Vaalhoek; BM = British Museum samples.

fluid can be produced by unmixing of a relatively low-salinity H_2O-CO_2 fluid, because the salt will fractionate into the H_2O-rich liquid phase rather than into the CO_2-rich vapor phase. If pressure varies widely during repeated crack-seal events (Sibson et al., 1988), then fluid entrapment during these events would reflect the changing position of the solvus resulting in variable H_2O/CO_2 proportions. Consequently, type 1_i, 1_{ii}, and 1_{iii} fluids are considered to be genetically related and formed from pressure-induced unmixing of the ore-bearing fluid during the principal period of gold and sulfide mineralization. However, we also recognize the relevance of limited fluid mixing, as is evident from the presence of a low-density carbonic phase in type 1 inclusions (Fig. 4). It is pertinent to note that the vertical veins are characterized by high-density CO_2 with a restricted range in T_h, whereas all horizontal veins exhibit a much broader range of CO_2 densities, implying a contribution of low-density basin-derived carbonic species.

The highly saline type 2 fluid inclusions, which are confined to the granite-hosted vertical veins, are similar to the high-salinity fluids recognized in granites of the Canadian Shield (Frape et al., 1984; Gascoyne et al., 1987) and Cornwall (Ed-

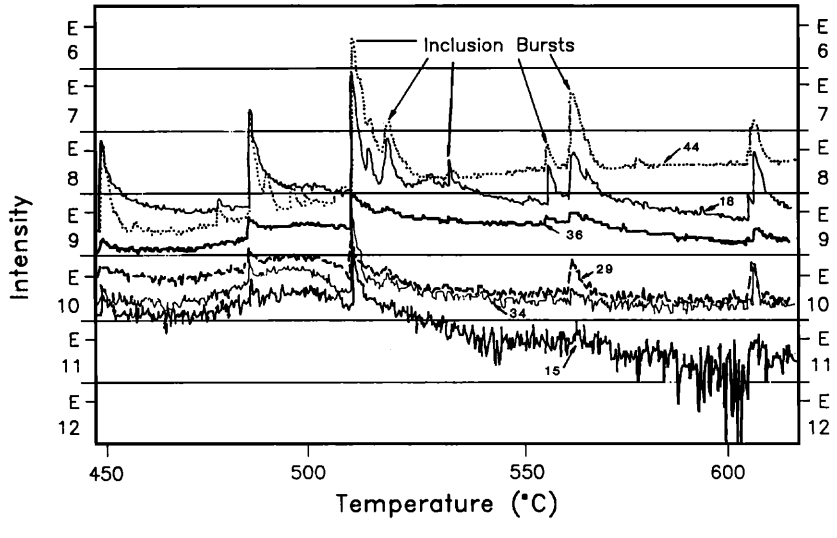

FIG. 8. Signal responses from quadrupole mass spectrometer analyses of individual fluid inclusion bursts from a native gold grain. Vertical scale is the negative logarithm of the SEM current. Horizontal scale indicates temperature (in °C) relative to the number of quadrupole mass spectrometer cycles. Masses monitored are identified in the diagram.

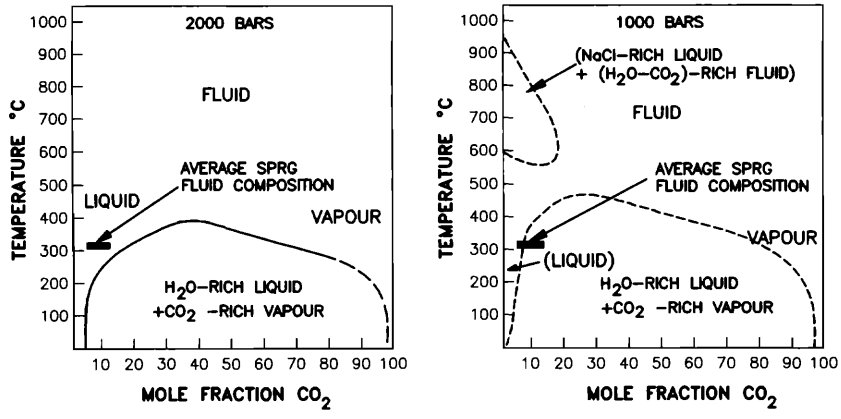

FIG. 9. T-X diagrams for 12 wt percent NaCl relative to H_2O + NaCl after Bowers and Helgeson (1983). Variations in pressure result in fluctuation of the solvus across the compositional field defined for the Sabie-Pilgrim's Rest gold field.

munds et al., 1984). The principal origins of the high salinity could be ascribed to acid hydrolysis of plagioclase, K feldspar, and biotite, but may also reflect evolved high-density basinal brines which are concentrated at the bottom of the Transvaal sub-basin as a result of their higher density.

Pressure and temperature estimates

The confining pressure of the Sabie-Pilgrim's Rest-type mineralization is not well constrained due to the lack of suitable geobarometers. Dissolution of daughter crystals after vapor homogenization indicates relatively high entrapment pressures, taking into account the limitations in interpretation emphasized by Roedder and Bodnar (1980). A reconstruction of the overburden at the time of quartz vein mineralization yields a thickness of approximately 7 to 8 km (Button, 1973, 1986) which corresponds to a lithostatic pressure of 2.2 to 2.5 kbars (at 1 kbar per 3.2 km using density data of Smit and Maree, 1966). This pressure estimate corresponds to an average fluid entrapment temperature of 320°C, using the Jacobs and Kerrick (1981) and Holloway (1981) equations of state to calculate isochores for the above fluid characteristics. The typical fluid composition used for these calculations involved a fluid with a salinity of 12 wt percent NaCl equiv and with a homogenization temperature between 170° and 200°C. By applying the above pressure correction to such a very typical fluid, entrapment temperatures of between 300° and 350°C are obtained. Furthermore, these temperatures correspond to those obtained using the arsenopyrite geothermometer of Lusk et al. (1993). Arsenopyrite from the Sabie-Pilgrim's Rest gold field contained As in the range 29.03 to 29.75 at. percent. A minimum estimate for the activity of sulfur was obtained from pyrite-pyrrhotite coexistence, yielding a log a_{S_2} value of −10.5. Using these figures, a temperature estimate of ±300°C is obtained, taking into account the limitations in accuracy of this geothermometer. This value is broadly compatible with values obtained by Anderson (1992), who presented As values that ranged between 28.8 and 31.7 at. percent ($\bar{x}$ = 30.5; n = 64; 1σ = 0.67), yielding a temperature range of 300° to 425°C ($\bar{x}$ = 375°C), assuming a a_{S_2} of −7.3. A third tenuous indication of mineralization temperatures is obtained from the coarse striated surfaces of vein-related pyrite, which suggests precipitation temperatures between 300° and 350°C.

Light stable isotopes

Quartz oxygen isotope data: Oxygen extraction from silicates were performed utilizing the conventional technique, using ClF_3 as reagent (Borthwick and Harmon, 1982; Vennemann and Smith, 1990), as well as the laser-based extraction method of Sharp (1990). Average NBS-28 values were used to convert the raw data to the V-SMOW scale using the accepted value of 9.64 per mil for NBS-28 (Coplen et al., 1983). The mean difference in $\delta^{18}O$ values of 23 NBS-28 samples was 0.12 per mil. NBS-30 yielded an average value of 5.1 per mil V-SMOW. All oxygen isotope values are reported in δ notation in per mil units relative to V-SMOW.

Thirty-two quartz samples from both the vertical and horizontal veins as well as the sill-dike-associated veins, covering a vertical stratigraphic span of approximately 1,000 m, were analyzed for oxygen isotope composition (Table 3). The vertical veins yielded a mean $\delta^{18}O$ = 14.2 per mil (σX = 0.34; n = 14), whereas the various horizontal veins have a slightly higher mean, $\delta^{18}O$ = 16.1 per mil (σX = 1.77; n = 48). Quartz from diabase sill-dike-associated deposits have average $\delta^{18}O$ = 20.7 per mil (σX = 1.23; n = 6). The data in Figure 10 demonstrate a distinct difference in ^{18}O content between carbonaceous sediment-and granite-hosted quartz veins. Variations in $\delta^{18}O$ values among the vertical quartz vein systems are tightly constrained (avg $\delta^{18}O$ = 14.3; σX = 0.3; n = 7), whereas the $\delta^{18}O$ values within individual horizontal veins vary (Table 3). Fluid $\delta^{18}O$ values were calculated from quartz mineral values for a 320°C equilibrium temperature using the equation of Matsuhisa et al. (1979; Table 3). These values ($\delta^{18}O_{fluid}$) range from 7.8 to 8.6 per mil for the vertical veins, from 5.3 to 12.9 per mil for the horizontal veins, and from 13.3 to 15.9 per mil for the dike-sill-associated deposits. All these values overlap with the range for both magmatic and metamorphic waters (5.5–9.0‰; Taylor, 1979).

Variations in the $\delta^{18}O$ values of hydrothermal quartz occur in response to a number of independent parameters. Quantitatively, the most important of these are the $\delta^{18}O$ value of the fluid and ambient temperature at which fluid-mineral

TABLE 3. Average $\delta^{18}O$ and $\delta^{18}O_{fluid}$ Values for Quartz from Vertical and Horizontal Veins as Well as Sill-Associated Gold Mineralized Localities (73 analyses)

Sample no.	$\Delta^{18}O$	$\delta^{18}O_{fluid}$	Sample no.	$\delta^{18}O$	$\delta^{18}O_{fluid}$
Horizontal veins			Vertical veins		
FKM075A	16.3 (15.7)	9.8	RFT113	14.8	8.6
FKM075B	14.7 (14.2)	8.3	SUN003	14.2	8.0
FKM076A	17.4	11.2	GRR099	14.2	8.0
FKM076B	17.2	11.0	GRR106	14.1	7.9
FKM077A	17.2	11.0	GRR107	14.2	8.0
FKM077B	16.5	10.3	GRR108	14.3	8.1
LJM090	14.0 (13.9)	7.8	AST109	14.0	7.8
NSM093	14.4 (14.1)	8.1			
BRH112	19.7	13.5	Sill-dike-associated veins		
MAM103	15.2	9.0			
MAM104	14.7	8.5	VLH040	22.1	15.9
CLH110	11.5	5.3	OGM082	19.5	13.3
CLH111	16.0	9.8	OGM083	20.1	13.9
BRH112	19.7	13.5			
MGL032	16.4	10.2			
MGL033	16.2	10.0			
CLS038	16.7	10.5			
JBH043	18.5	12.3			
DRM044	19.1	12.9			
GLS052	16.6	10.4			
CLW013	16.7	10.5			
CLW017	17.8 (17.8)	11.6			
THH030	15.4	9.2			

Values in parentheses were generated using the laser ablation method of extraction; $\delta^{18}O_{fluid}$ values were calculated from quartz mineral values using the quation of Matsuhisa et al. (1979) for T = 320°C; all values are expressed in per mil notation relative to V-SMOW

Locality abbreviations: AST = Astra, BRH = Browns Hill, CLW = Clewer West, CLS = Clewer South, DRM = Desiree, FKM = Frankfort, GLS = Glynns Lydenburg Sheba, GRR = Gregory, JBH = Jubilee, LJM = Little Joker, MAM = Mamre, MGL = Morgenzon, NSM = Nestor, OGM = Olifantsgeraamte, RFT = Rietfontein, SUD = Sudwala, SUN = Sunlight, THH = Theta Hill; VLH = Vaalhoek

isotopic equilibrium is attained (Kerrich, 1987). At the site of mineralization, the $\delta^{18}O$ values of hydrothermal fluids may be modified by (1) exchange reactions with the wall rock, (2) precipitation or solution of an oxygen-bearing phase either depleted or enriched in ^{18}O with respect to the fluid, (3)

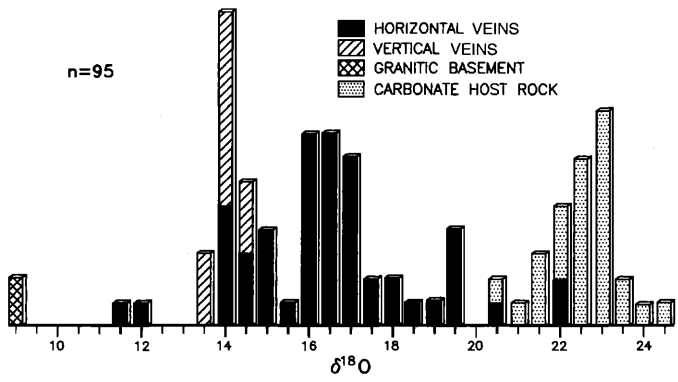

FIG. 10. $\delta^{18}O$ values for quartz separates from various Au-bearing veins in the Sabie-Pilgrim's Rest gold field. Values for the carbonaceous host rocks are from Schidlowski et al. (1975). All values are presented in per mil notation, relative to V-SMOW.

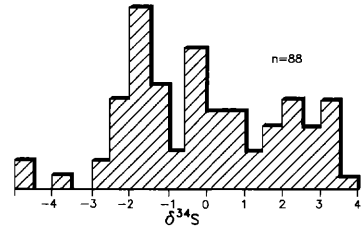

FIG. 11. $\delta^{34}S$ values for pyrite separates from gold-bearing quartz veins in the Sabie-Pilgrim's Rest gold field. All values are expressed in per mil notation relative to Canyon Diablo troilite (CDT).

separation of an immiscible CO_2 phase, or (4) mixing with an isotopically distinct fluid. An inconsistent variation in $\delta^{18}O$ with decreasing depth suggests ^{18}O contributions from an external oxygen source or decreasing temperature. A strong lithological control (option 1 above) on $\delta^{18}O$ values in the Sabie-Pilgrim's Rest gold field is evident in Figure 10, with low values for the granite-hosted veins, higher values for the veins hosted in the overlying dolomite, and the highest $\delta^{18}O$ values associated with diabase dikes-sills. The data compare favorably with the oxygen isotope values presented by Tyler (1986; $\delta^{18}O$ = 12.1–19.5‰) and Anderson (1992; $\delta^{18}O$ = 10.4–19.8‰). The $\delta^{18}O$ values obtained by Tyler (1986) for the strata-bound veins of the Malmani Subgroup cluster between 17 and 18 per mil, whereas the vertical veins yielded slightly lower values, ranging between 14.1 and 15.2 per mil. The $\delta^{18}O$ values for the veins in the siliciclastic Pretoria Group exhibit the heaviest isotope compositions, varying between 12.1 and 14.4 per mil. These low $\delta^{18}O$ values for the Pretoria Group-hosted veins were confirmed by Anderson (1992) who reported compositions ranging between 10.4 and 13.9 per mil. Clastic sedimentary rocks (shales) from the Black Reef Formation yielded $\delta^{18}O$ values ranging from 7.5 to 10.6 per mil (Shieh and Zhang, 1988). Schidlowski et al. (1975) have shown that the oxygen isotope composition of dolomite in the vicinity of the Sabie-Pilgrim's Rest gold field ranges between 21.5 and 22.9 per mil, whereas $\delta^{18}O$ values of the carbonate gangue phases (dolomite and calcite) vary between 16.1 and 21.5 per mil. Schiffries and Rye (1989) have also presented $\delta^{18}O$ values of 20 ± 1 per mil for dolomite from the Malmani Subgroup, whereas the intrusive rocks from the Bushveld Complex yielded average $\delta^{18}O$ values of 7.2 ± 0.4 per mil for plagioclase, 6.6 ± 0.2 per mil for orthopyroxene, and 6.9 ± 0.2 per mil for the average melt composition. The observed variations in $\delta^{18}O$ values of vein quartz from different stratigraphic heights in the Sabie-Pilgrim's Rest gold field strongly argue that wall-rock interaction largely controlled the oxygen isotope composition. Variations within stratiform quartz veins probably result from a combination of immiscibility of CO_2 and mixing with a fluid of distinct isotopic composition.

Pyrite sulfur isotope data: Sulfur in pyrite was converted to SO_2 using the Cu_2O oxidation method of Coleman and Moore (1978). Sixty pyrite samples from within the horizontal quartz veins were analyzed for $\delta^{34}S$. They yielded a range from −4.6 to 3.3 per mil (Fig. 11), which agrees with the small number of analyses presented by Tyler (1986). The stratigraphically lower vein horizons are characterized by $\delta^{34}S$

TABLE 4. Light Stable Isotope Values (δD, δ^{13}C, and δ^{18}O) of Extracted Inclusion Fluids from Horizontal Veins (Clewer West = CLW), Vertical Veins (Gregory = GRR and Rietfontein = RFT), and Sill-Associated Veins (Olifantsgeraamte = OGM)

Sample no.	δD_{H_2O}	$\Delta^{13}C_{total}$	$\delta^{18}O_{fluid}$
OGM082	−47	−11.7	13.3
GRR107	−37	−2.8	8.0
CLW017	−53	−10.8	11.6
RFT001	−68	−4.8	6.5°
CLW017	−54	−1.4	15.4°
RFT113	−61	−5.7	8.6
CLW013	−47	−4.1	10.5
VLH040	−36	−0.3	15.9
FKM075A	−58	−8.2	9.8
MAM104	−17	−6.1	8.5
MGL033	−49	−8.4	10.0
GRR107	−47	−12.0	8.0
BRH112	−16	1.8	13.5

Data are presented relative to per mil V-SMOW; $\delta^{18}O$ values are calculated from $\delta^{18}O_{quartz}$ using the equation of Matshuhisa et al. (1979) for T = 320°C; ° = values from pyrite-hosted fluid inclusions

values for pyrite ranging from 3.3 to −1.2 per mil, characteristic of magmatic sulfur. The upper veins have more negative δ^{34}S values, ranging from 1.9 to −4.6 per mil, which coincides with the trend toward negative δ^{34}S numbers in sulfides from host-rock sediments (Cameron, 1982). Cameron (1982) identified an isotopic transition zone in the lower Malmani Subgroup, above which sulfides from intercalated shales were derived from sulfate reduction, involving both biogenic and inorganic processes. Liebenberg (1968) determined the sulfur isotope composition of a large number of host-rock samples from the Transvaal Supergroup, with values covering a wide range between −11.6 to 7.8 per mil.

Fluid inclusion stable isotope data: Measurements of δD and δ^{13}C were performed on fluids from decrepitated fluid inclusions in selected quartz and pyrite samples, following the method described by Vennemann and O'Neil (1993). These data are presented in Table 4. The hydrogen isotope composition of water in quartz-hosted fluid inclusions is variable and extends from −61 to −16 per mil. This wide range in values cannot be accounted for by mixing of fluids from depleted and enriched δD fluid reservoirs because any such mixing would be reflected in shifts of both δD and $\delta^{18}O_{fluid}$, which is inconsistent with the relatively uniform $\delta^{18}O_{fluid}$ values. Rather, the observed range in δD may also be due to the variable presence of H_2 and/or CH_4 in the aqueous fluid, as confirmed by the gas chemistry data (Table 1). When plotted on a δ^{18}O vs. δD diagram (Fig. 12), the Sabie-Pilgrim's Rest data coincide with the primary magmatic and metamorphic water fields, and show no indication of any isotopic interaction with meteoric water. The fluid δD and $\delta^{18}O_{fluid}$ data are inconclusive with regard to the origin of the ore-bearing fluid, and cannot be used to discriminate between the involvement of meteoric-, metamorphic-, magmatic-, and/or basinal-derived fluids. However, the Sabie-Pilgrim's Rest δD and δ^{18}O data are distinctly different from those of fluids in epithermal, volcanic-associated massive sulfide and Mississippi Valley-type deposits (e.g., Ohmoto, 1986).

Carbon isotope values for fluid inclusions range from 1.8 to −12.0 per mil. Schidlowski et al. (1975) determined the average δ^{13}C value of carbonate minerals from the Sabie-Pilgrim's Rest gold field veins to be around −2.4 per mil. These data suggest that hydrothermal fluids may have acquired carbonic species (CO_2, H_2CO_3, HCO_3^- from the carbonate host rocks. Under conditions where pressure equals 2.2 to 2.5 kbars and temperature = 320°C, the $\delta^{13}C_{Ca,Mg(CO_3)_2} \approx \delta^{13}C_{fluid}$ (Ohmoto and Rye, 1979), and fractionation between oxidized carbon species CO_3^{2-}, H_2CO_3) in solution is small (Bottinga, 1969). The calcite-HCO_3^- fractionation is ~1 per mil at 320°C (Kyser, 1987), so that calcite of −3 per mil would have been precipitated from a fluid with $\delta^{13}C$ $HCO_3^- \approx -4$ per mil. Although the δ^{13}C values of aqueous carbonate depend on a number of factors, the observed range in δ^{13}C for samples from the Sabie-Pilgrim's Rest gold field suggest that carbon species could have been acquired during dissolution and decarbonatization of the host dolomitic rocks.

In summary, the uniformity of the δ^{18}O values of quartz in individual horizontal and vertical vein deposits implies a consistent ambient temperature. Furthermore, a dominant lithological control on the δ^{18}O and δ^{34}S values is apparent. Such an interpretation could explain the irregular variations in δ^{18}O throughout the stratigraphic sequence. The shift toward negative δ^{34}S values in vein-associated sulfides could also be ascribed to isotopic exchange with sulfides derived from sulfate reduction within intercalated shales, thereby confirming the lithologic control on stable isotope compositions. The significant lithological control of the host rock on the stable isotope compositions, and the lack of knowledge on the extent of fluid-rock interaction, prevents determination of the original stable isotope composition of the mineralizing fluid.

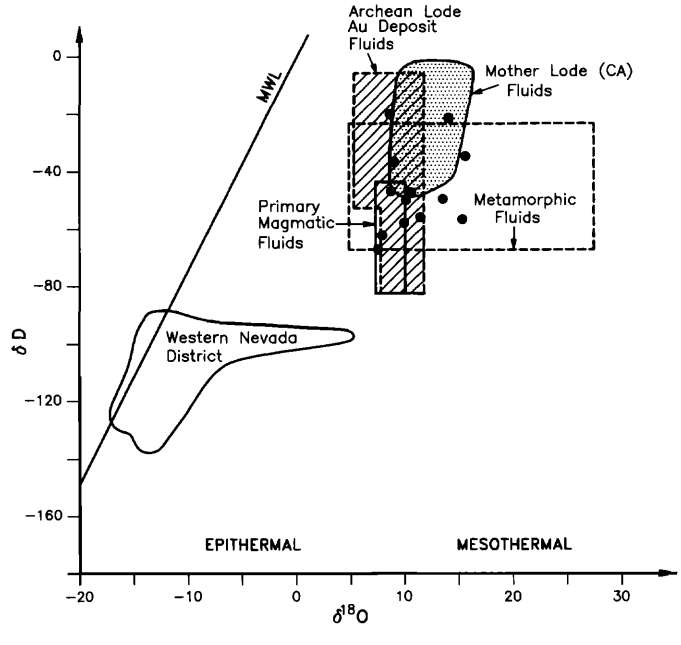

FIG. 12. A δD vs. δ^{18}O plot depicting the stable isotope geochemistry of Sabie-Pilgrim's Rest ore-bearing fluids. MWL = meteoric water line (modified after O'Neil and Silberman, 1974, and Sheppard, 1986.

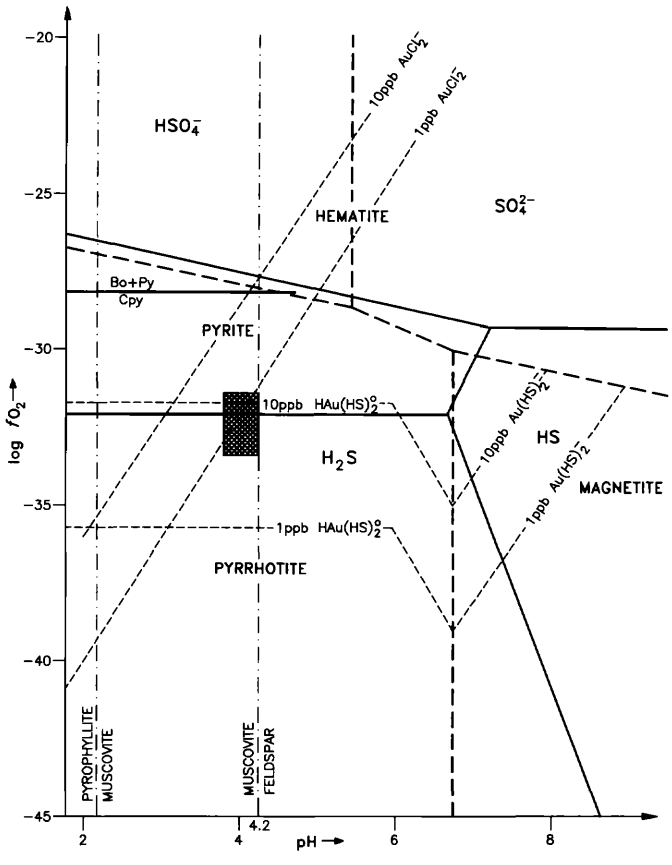

FIG. 13. Composite log f_{O_2} versus pH diagram for Sabie-Pilgrim's Rest conditions. Calculated using SUPCRT92 (Johnson et al., 1992). Shaded area represents an approximation of activities of vein forming fluids, based on average quadrupole mass spectrometer gas analytical results.

Transport and Deposition of Ore

Data presented in this study allow the following summation to be made regarding the mineralizing fluid which formed the Sabie-Pilgrim's Rest deposits. Mineralization formed at a mean temperature of around 320°C and a pressure of 2.2 to 2.5 kbars; the average mole fraction carbonic species in the fluids was about 0.05 as determined by the quadrupole mass spectrometer gas analyses, and fluid salinities range from 5.5 to 23.5 wt percent NaCl equiv with an average of ≈12 wt percent NaCl equiv, as indicated by $T_{m_{ice}}$ measurements. Activities of ionic species in this fluid were log $a_{Na} = -1.08$, log $a_K = -0.32$, and log $a_{Cl} = -0.27$, with an ionic strength = 2.46 and an Na/K ratio of 0.1 (Harley, 1993; Boer and Harley, 1994). In terms of the reaction muscovite + $6K^+$ + 6 quartz ⇄ 3K feldspar + $2H^+$ (log $K = -7.919$; calculated using SUPCRT92, Johnson et al., 1992), an acidic pH (neutral pH = 5.1 at 320°C) is indicated for the Sabie-Pilgrim's Rest fluids, because no K feldspar was observed (Boer and Harley, 1994). Redox conditions are constrained by sulfide-phase stability fields, calculated for the specific thermodynamic conditions specified above (Fig. 13).

Using these fluid characteristics, inferences on the gold speciation and precipitation mechanism is possible. Experimental data on Au bisulfide complexes (Seward, 1973; Shenberger and Barnes, 1989; Hayashi and Ohmoto, 1991) for the conditions outlined above indicate solubilities of between 1 and 10 ppb. Calculations of Au chloride complex solubility for Sabie-Pilgrim's Rest gold field conditions, using data of Henley (1973) and Shenberger and Barnes (1989), yield values of similar magnitude (Fig. 13). This implies that Sabie-Pilgrim's Rest gold could have been transported equally efficiently as either a bisulfide or a chloride complex. The possible significance of the chloride complex may also explain the preponderance of Cu mineralization in the Sabie-Pilgrim's Rest gold field compared to other mesothermal lode gold deposits, since Cu is efficiently transported as a chloride complex. Precipitation mechanisms pertinent to a fluid transporting gold as a bisulfide complex include a decrease in T at constant pH, oxidation of the complex, pH reduction, and reduction in sulfur activity in the fluid by sulfide precipitation. Oxidation may be ruled out as a first-order control in gold precipitation because fluid CO_2/CH_4 ratios remain relatively constant throughout the Sabie-Pilgrim's Rest gold field. This situation differs from that at the Pamour mine in the Timmins district in Canada, for example, where widely variable CO_2/CH_4 ratios have been taken as an indication of the influence of changing oxidation states on gold precipitation (Walsh et al., 1988). Given the strong association of gold with various sulfides noted at many mines in the Sabie-Pilgrim's Rest gold field (Meyer et al., 1986; Harley and Charlesworth, 1992), the role of sulfide precipitation may have been important for gold precipitation. However, as indicated by gas analyses from gold-hosted fluid inclusions, phase separation was an important process during fluid evolution and may be the principal controlling mechanism for both gold and sulfide precipitation. In all likelihood gold precipitation was mainly controlled both by a decrease in sulfur activity within the ore-bearing fluid because of sulfide precipitation and by changes in the fluid chemistry as a result of fluid immiscibility. The fact that gold in the Sabie-Pilgrim's Rest gold field occurs in several ways probably supports the view that at least two mechanisms applied to metal precipitation. In the Sabie-Pilgrim's Rest gold field, gold occurs (1) primarily as fracture fills within early sulfides (e.g., Elandshoogte, Clewer West, Malieveld), (2) as round cogenetic inclusions within sulfides, mainly pyrite (e.g., Olifantsgeraamte, Vaalhoek), and (3) as free gold within quartz (e.g., Morgenzon). All three styles of gold occurrence can be found within a single deposit, implying that different mechanisms of precipitation may have occurred even locally. It also cannot be ruled out that gold in late fractures was precipitated as a result of adsorption-reduction reactions (Bancroft and Hyland, 1990; Schoonen et al., 1992).

Sabie-Pilgrim's Rest Gold Field in Relation to Other Mesothermal Gold Deposits

Mesothermal gold deposits can be classified into mainly three types: (1) greenstone hosted (Superior province, Canada; Yilgarn and Pilbara cratons, Western Australia; Kaapvaal and Zimbabwian cratons, southern Africa), (2) turbidite hosted (Victoria, Australia; Nova Scotia, Canada), and (3) cordilleran vein-type deposits (felsic intrusion related). Low pressures (less than 3 kbars) are generally inferred for these mesothermal deposits, with temperatures around 300° to 400°C.

Characteristic features of the Sabie-Pilgrim's Rest gold

field that correspond to those within the above spectrum of mesothermal gold deposits include: (1) comparable light stable isotope ranges, together with a lack of isotopic evidence for unmodified meteoric water involvement; (2) high Au/Ag ratios; (3) presence of ore shoot structures, which are highly characteristic of mesothermal gold deposits (Colvine et al., 1984); (4) variably deformed structures within individual sheeted veins (Harley and Charlesworth, 1995), which point toward cyclic opening and quartz accretion events separated by episodes of deformation; and (5) fluid inclusion properties, which indicate high fluid pressures during entrapment. However, several features also distinguish the Sabie-Pilgrim's Rest ores from typical mesothermal deposits: (1) the Sabie-Pilgrim's Rest gold field is spatially associated with a large layered mafic intrusion, the Bushveld Complex, and overlies one of the two concentric structures along which feeder sites to the Bushveld Complex (such as Losberg and Uitkomst) are arranged (Sharpe et al., 1981)—furthermore, the age of gold mineralization is broadly coeval with the emplacement age of the Bushveld Complex; (2) veins are largely hosted within a platform carbonate sequence; (3) salinities are high (mean ≈12 wt % NaCl equiv); (4) mean bulk CO_2 content is low (≈5 mole %); and (5) ubiquitous Cu, Bi, and lesser W in addition to Au, Ag, As, and Sb sulfides are present.

Genesis of the Sabie-Pilgrim's Rest Gold Field Ores

Deposition of the Sabie-Pilgrim's Rest gold field ores is constrained between the emplacement of pre-Bushveld-aged diabase intrusions which have been metamorphosed and then cut by mineralized vein systems, and unmetamorphosed pyroxenitic dikes, thought to be related to the Main zone of the Rustenburg Layered Suite, which transgress mineralization. The Bushveld Complex was intruded over a relatively brief interval between 2061 ± 27 Ma (Rustenburg Layered Suite; Walraven et al., 1990) and 2054.4 ± 1.8 Ma (Lebowa Granite Suite; Walraven and Hattingh, 1993). Deposition of the Sabie-Pilgrim's Rest gold field ores is probably, therefore, broadly coeval with the early stages of emplacement of the Bushveld Complex.

Besides its contemporaneity with the Bushveld igneous event, the Sabie-Pilgrim's Rest gold field is also spatially related to the complex. The gold field occurs over a restricted area (ca. 10^3 km^2) of the Transvaal sub-basin and, although several other small hydrothermal occurrences of gold are developed elsewhere in the Transvaal sub-basin, this is by far the most important mineralized section. It lies some 40 to 50 km east of the present limit of the Bushveld Complex but is situated on or close to two major concentric fracture zones which encompass and control the emplacement of the Bushveld Complex and its satellites (Sharpe et al., 1981). The smaller Mamre-Slaaihoek gold field, for example, to the south of the Sabie-Pilgrim's Rest gold field (Fig. 1), is spatially associated with the Uitkomst intrusion, a Bushveld Complex satellite that also occurs on one of the concentric fractures which encircle the complex. It is not known with certainty whether a mafic intrusion exists beneath the Sabie-Pilgrim's Rest gold field, although geophysical indications suggest the presence of a number of magnetic anomalies in the general area of the gold (P.N. Bentley, pers. commun., 1994). These anomalies may be related to the presence of mafic intrusions at depth beneath the Transvaal sediments.

The occurrence of mineralized veins in the Sabie-Pilgrim's Rest gold field is observed at irregular intervals over at least 1,000 m of vertical extent, from the steeply dipping lodes in the granite basement beneath the Transvaal sedimentary cover, to flat-lying lodes well up into the Pretoria Group (Fig. 1). The nature of the fluids that are associated with the deposition of this extensively mineralized system are heterogeneous but appear to have been derived at least partially from a deep-seated source. The hydrothermally altered diabasic wall rock at the Olifantsgeraamte mine is characterized by an enhanced radiogenic Sr isotope signature ($^{87}Sr/^{86}Sr$ = 0.752–0.769) relative to unaltered diabase ($^{87}Sr/^{86}Sr$ = 0.715–0.729), suggesting that the hydrothermal fluids themselves were enriched in ^{87}Sr. This supports the suggestion that the fluids interacted with a relatively high Rb/Sr rock such as the Nelspruit porphyritic granite (Rb typically 100–200 ppm, Sr typically 300–500 ppm) which occurs beneath the Sabie-Pilgrim's Rest gold field. Furthermore, type 2 fluids, with low X_{CO_2} and high salinities, occur largely with the vertical granite-hosted veins in the Sabie-Pilgrim's Rest gold field, whereas the compositionally diverse type 1 fluids occur throughout the mineralized successions. This pattern of fluid distribution indicates that the fluid chemistry reflects interaction with the host-rock lithology but is also consistent with derivation of type 2 fluids from a deep-seated, possibly an original magmatic, source, with incursion of this fluid into the host rocks during upward flow through the granite basement into the overlying sedimentary sequences. Oxygen and sulfur isotope compositions clearly point to variable values which tend to range between the extremes of pristine juvenile signatures and values consistent with fluid-rock interaction. Quadrupole mass spectrometer gas analysis on quartz-hosted inclusion fluids indicate that carbonate-hosted veins have higher CO_2 and CH_4 abundances than, for example, the vertical granite-hosted veins, confirming the influence of host rock on fluid composition. Low N_2/Ar ratios, as well as $\delta^{18}O$ and δD values, in the Sabie-Pilgrim's Rest gold field ore fluids suggest negligible interaction with a meteoric fluid component. However, we are not able to evaluate quantitatively the proportional contribution of fluid sources from either magmatic or sedimentary brines to the Sabie-Pilgrim's Rest gold field hydrothermal system.

Mineralization in the Sabie-Pilgrim's Rest gold field was stimulated by a deep-seated heat source which initiated convective overturning of originally pristine juvenile fluid-transporting metals that were probably derived from the same source, as well as by a measure of connate waters. The reconstituted remnants of such fluids are now preferentially preserved in the vertical granite-hosted vein systems. This fluid was relatively acidic and anoxic and equally efficient in transporting gold as either a bisulfide complex or a chloride complex, whereas copper may have been in solution as a chloride complex. The volumetrically dominant Sabie-Pilgrim's Rest gold field ore fluid (type 1), however, has been significantly modified by local fluid-rock interaction and is now represented by a fluid inclusion population exhibiting a variable continuum of H_2O/CO_2 ratios and salinities. These characteristics are confirmed by quantitative quadrupole mass spec-

trometer gas analyses. The fluid population is believed to have been derived by fluid unmixing that was initiated by periodic depressurization associated with crack-seal events in a fault-valve system formed by bedding plane slip during Bushveld-related structural adjustments in the Transvaal subbasin. Periodic CO_2 effervescence associated with this unmixing event may have been responsible for a large measure of metal precipitation, especially the abundant native gold in quartz present in the Sabie-Pilgrim's Rest gold field. Fluid overpressures were instigated by the shale-rich cap rocks of the Pretoria Group, covering the more permeable carbonate sediments of the Chuniespoort Group. Phase separation was an important process during fluid evolution and is thought to be the principal controlling mechanism for both gold and sulfide precipitation. Gold precipitation was mainly controlled both by a decrease in sulfur activity within the ore-bearing fluid because of sulfide precipitation and changes in the fluid chemistry as a result of fluid immiscibility.

The Sabie-Pilgrim's Rest gold field is a predominantly sediment-hosted, Au-Cu-(Bi-As-Sb-W) metal province that represents an unusual member in the family of mesothermal ore deposits. As recognized in the past and confirmed in this study, the characteristics of the gold field appear to be related to its close spatial, temporal and genetic association with the Bushveld Complex and its satellites. The minimum fluid volume required to account for all the gold (168 tons) in the gold field is approximately 1.68×10^{13} l which, assuming a gold solubility of 10 ppb, could be derived from a Bushveld-type magma only 560 km^3 in size. Schiffries and Skinner (1987) have shown that the Bushveld hydrothermal system has affected tens of thousands of cubic kilometers of rock, which rates it among the largest paleo-hydrothermal systems in the world. Numerous Bushveld-related satellite intrusions of this magnitude exist in the central Kaapvaal craton and, given the geophysical evidence, it is tempting to suggest that such an intrusion might be linked genetically to the formation of the Sabie-Pilgrim's Rest gold field. A relationship between mesothermal Au-Cu deposits and hidden or distant mafic-felsic intrusions has obvious exploration significance, not only to the vast expanse of Transvaal sediments on the Kaapvaal craton, but also to similiar geologic settings elsewhere in the world.

Conclusions

The hydrothermal deposits of the Sabie-Pilgrim's Rest gold field are unusual in terms of geologic setting and geochemical characteristics, and do not correspond to any of the known genetic models for typical mesothermal deposits. This study of the Sabie-Pilgrim's Rest gold field has indicated the following:

1. Age constraints indicate that gold mineralization in the Sabie-Pilgrim's Rest gold field is concurrent with the emplacement age of the Bushveld Complex.

2. Mineralization occurred at temperatures around 320°C, at pressures in the range of 2.2 to 2.5 kbars, and at depths of 7 to 8 km. Vein textures indicate the involvement of high-pressure (supralithostatic) fluids.

3. Oxygen isotope values of quartz from the vertical veins are remarkably consistent (avg $\delta^{18}O$ = 14.2‰) and are significantly different from those of the horizontal veins (avg $\delta^{18}O$ = 16.1‰) and sill-dike-associated veins (avg $\delta^{18}O$ value of 20.7‰). The $\delta^{34}S$ values of vein pyrite range from −2.8 to +3.1 per mil. The δD, $\delta^{18}O$, and $\delta^{13}C$ values from inclusion fluids (δD_{quartz} = −37 to −53‰; $\delta^{18}O_{pyrite}$ = −54 to −68‰; $\delta^{18}O$ = 6.5 to 15.4‰; $\delta^{13}C$ = −11.7 to −1.4‰) coincide predominantly with values of primary magmatic and/or metamorphic water and exclude the involvement of meteoric water. Stable isotope data clearly suggest interaction of the ore fluid with the host rocks, and changes in stable isotope composition are largely host-rock dominated.

4. The nature of the ore-bearing fluid was predominantly aqueous, with <5 mole percent carbonic species. Other gases, mainly CH_4, C_2H_6, N_2, Ar, H_2S, SO_2, and HCl, were present in abundances <1 mole percent. The strata-bound veins contain significantly higher concentrations of CO_2 and CH_4 as opposed to the Ar- and HCl-rich vertical veins. The higher abundances of carbonic gas species (CO_2 and CH_4) in the carbonate-hosted veins suggest decarbonatization of the dolomitic host rock by interaction with the hydrothermal fluid, as well as thermocatalysis of shale-hosted organic matter. However, the higher CO_2 and CH_4 contents in the upper veins could also be a direct result of H_2O-CO_2 phase separation. Evidence for phase separation is suggested by quadrupole mass spectrometer results from individual native gold-hosted fluid inclusions, showing varying CO_2/H_2O ratios. High HCl concentrations in vertical veins correlate well with high salinities. The gaseous contents of the veins, to some extent, reflect the host rock lithologies.

5. The ore-bearing solutions were reducing ($f_{O_2} \approx 10^{-32.5}$) and the activity of the H_2S species was between $10^{-2.5}$ and $10^{-2.8}$. Furthermore, the ore fluids were acidic with salinities ranging between 5.5 and 23.5 wt percent NaCl equiv for the horizontal veins and ≈30 wt percent NaCl equiv for the vertical veins.

6. Gold was equally soluble as a bisulfide complex or a chloride complex. Gold precipitation was enhanced by several mechanisms, including lowering of sulfur activity due to precipitation of sulfide minerals, changes in fluid chemistry due to unmixing within the fluid phase, and limited interaction with the sedimentary host rock. However, the dominant mechanism for gold precipitation was phase separation, as indicated by quadrupole mass spectrometer results as well as by fluid inclusion petrography. Different styles of gold occurrence confirm that several mechanisms of precipitation may have been active, which makes the prediction of the siting of gold with respect to the vein components very difficult on a regional scale.

7. The Sabie-Pilgrim's Rest gold field proved to be a different type of mesothermal gold deposit, possibly associated with a layered basic igneous complex, the Bushveld Complex. In view of the widespread nature of such mafic complexes, such an association could be significant in terms of opening new exploration targets.

Acknowledgments

The authors thank Randgold and Exploration Company Ltd., particularly Phil Bentley, for financial and logistic assistance. Conventional oxygen isotope analyses on quartz samples were performed at the Department of Geological Sci-

ences, University of Cape Town, with the help of Chris Harris; sulfur isotopes were analyzed at the Schonland Research Centre for Nuclear Sciences, University of the Witwatersrand; and other stable isotope analyses, as well as quadrupole mass spectrometer analyses of inclusion fluids, were performed in the laboratories of James O'Neil and Stephen Kesler, respectively, at the Department of Geological Sciences at the University of Michigan. Many discussions with Robert Bodnar, Michael Harley, Phil Bentley, and Ed van Hees are gratefully acknowledged. BM samples were obtained from the British Museum (Natural History), London, with the help of Chris Stanley. We thank Chris Harris and Hartwig Frimmel for their constructive reviews which improved the quality of the manuscript. This work was partially sponsored by the National Geosciences Programme of the South African Foundation for Research Development and formed part of R.H.B.'s Ph.D. project.

June 15, 1994; January 17, 1995

REFERENCES

Anderson, M.R., 1992, A fluid inclusion and isotopic study of gold-bearing veins in the Transvaal Sequence, South Africa: Unpublished Ph.D thesis, London, University of London, 276 p.

Anderson, M.R., Rankin, A.H., and Spiro, B., 1992, Fluid mixing in the generation of mesothermal gold mineralisation in the Transvaal Sequence, Transvaal, South Africa: European Journal of Mineralogy, v. 4, p. 933–948.

Ash, J.P., and Tyler, N., 1986, A preliminary investigation of fluid-inclusions in the Pilgrim's Rest gold field, eastern Transvaal: University of the Witwatersrand, Economic Geology Research Unit Information Circular, v. 180, 21 p.

Bancroft, G.M., and Hyland, M.M., 1990, Spectroscopic studies of adsorption/reduction reactions of aqueous metal complexes on sulphides surfaces: Reviews in Mineralogy, v. 23, p. 511–558.

Bodnar, R.J., 1993, Revised equation and table for determining the freezing-point depressions of H_2O-NaCl solutions: Geochimica et Cosmochimica Acta, v. 57, p. 683–684.

Boer, R.H., and Harley, M., 1994, "Fluid mixing and the generation of mesothermal gold mineralisation in the Transvaal Sequence, Transvaal, South Africa"—a discussion: European Journal of Mineralogy, v. 6, p. 419–421.

Borthwick, J., and Harmon, R.S., 1982, A note regarding ClF_3 as an alternative to BrF_5 for oxygen isotope analysis: Geochimica et Cosmochimica Acta, v. 46, p. 1665–1668.

Bottinga, Y., 1969, Calculated fractionation factors for carbon and hydrogen isotope exchange in the system calcite-carbon dioxide-graphite-methane-hydrogen-water vapor: Geochimica et Cosmochimica Acta, v. 33, p. 49–64.

Bowers, T.S., 1991, The deposition of gold and other metals: Pressure-induced fluid immiscibility and associated stable isotope signatures: Geochimica et Cosmochimica Acta, v. 55, p. 2417–2434.

Bowers, T.S., and Helgeson, H.C., 1983, Calculations of the thermodynamic and geochemical consequences of nonideal mixing in the system H_2O-CO_2-NaCl on phase relations in geologic systems: Equation of state for H_2O-CO_2-NaCl fluids at high pressures and temperatures: Geochimica et Cosmochimica Acta, v. 47, p. 1247–1275.

Boxall, W.P., 1938, The Rietfontein (TCL) mine, Sabie: Chemical, Metallurgical and Mining Society of South Africa Journal, v. 39, p. 84–102.

Button, A., 1973, A regional study of the stratigraphy and development of the Transvaal basin in the eastern and northeastern Transvaal: Unpublished Ph.D. thesis, Johannesburg, University of the Witwatersrand, 282 p.

——1986, The Transvaal sub-basin of the Transvaal Sequence, *in* Anhaeusser, C.R., and Maske, S., eds., Mineral deposits of southern African: Johannesburg, Geological Society of South Africa, p. 811–817.

Cameron, E.M., 1982, Sulphate and sulphate reduction in early Precambrian oceans: Nature, v. 296, p. 145–148.

Cheney, E.S., and Twist, D., 1991, The conformable emplacement of the Bushveld mafic rocks along a regional unconformaty in the Transvaal succession of South Africa: Precambrian Research, v. 52, p. 115–132.

Clendenin, C.W., Jr., 1989, Tectonic influence on the evolution of the Early Proterozoic Transvaal Sea, southern Africa: Unpublished Ph.D. thesis, Johannesburg, University of the Witwatersrand, 347 p.

Coleman, M.L., and Moore, M.P., 1978, Direct reduction of sulphates to sulphur dioxide for isotopic analysis: Analytical Chemistry, v. 50, p. 1594–1595.

Colvine, A.C., Andrews, A.J., Cherry, M.E., Durocher, M.E., Fyon, A.J., Lavigne, M.J., Jr., Macdonald, A.J., Marmont, S., Poulsen, K.H., Springer, J.S., and Troop, D.G., 1984, An integrated model for the origin of Archean lode gold deposits: Ontario Geological Survey Open-File Report, v. 5524, 98 p.

Coplen, T.B., Kendall, C., and Hopple, J., 1983, Comparison of stable isotope reference samples: Nature, v. 302, p. 236–238.

Dowling, K., and Morrison, G., 1989, Application of quartz textures to the classification of gold deposits using North Queensland examples: ECONOMIC GEOLOGY MONOGRAPH 6, p. 342–355.

Edmunds, W.M., Andrews, J.N., Burgess, W.G., Kay, R.L.F., and Lee, D.J., 1984, The evolution of saline and thermal groundwaters in the Carnmenellis granite: Mineralogical Magazine, v. 48, p. 407–424.

Fowler, A.R.C., 1968, Mining at Transvaal Gold Mining Estates, Limited 1872–1967: South African Institute of Mining and Metallurgy Journal, v. 68, p. 291–335.

Frape, S.K., Fritz, P., and McNutt, R.H., 1984, Water-rock interaction and chemistry of groundwaters from the Canadian Shield: Geochimica et Cosmochimica Acta, v. 48, p. 1617–1627.

Gascoyne, M., Davison, C.C., Ross, J.D., and Pearson, R., 1987, Saline groundwaters and brines in plutons in the Canadian Shield: Geological Assocaition of Canada Special Paper 33, p. 53–68.

Harley, M., 1993, The geology of the Sabie-Pilgrim's Rest goldfield with special reference to the Elandshoogte mine: Unpublished Ph.D. thesis, Johannesburg, University of the Witwatersrand, 286 p.

Harley, M., and Charlesworth, E.G., 1992, Thrust-controlled gold mineralization at the Elandshoogte mine, Sabie-Pilgrim's Rest goldfield, South Africa: Mineralium Deposita, v. 27, p. 122–128.

——1955, The role of fluid pressure in the formation of bedding parallel, thrust-hosted gold deposits, Sabie-Pilgrim's Rest goldfield, eastern Transvaal: Precambrian Research.

Hayashi, K.-I., and Ohmoto, H., 1991, Solubility of gold in NaCl-and H_2S-bearing aqueous solutions at 250–350°C: Geochimica et Cosmochimica Acta, v. 55, p. 2111–2126.

Henley, R.W., 1973, The solubility of gold in hydrothermal chloride solutions: Chemical Geology, v. 11, p. 622–635.

Holloway, J.R., 1981, Compositions and volumes of supercritical fluids in the earth's crust: Mineralogical Association of Canada Short Course Handbook, v. 6, p. 13–38.

Jacobs, G.K., and Kerrick, D.M., 1981, Methane: An equation of state with application to the ternary system H_2O-CO_2-CH_4: Geochimica et Cosmochimica Acta, v. 45, p. 607–614.

Johnson, J.W., Oelkers, E.H., and Helgeson, H.C., 1992, SUPCRT92: A software package for calculating the standard molal thermodynamic properties of minerals, gases, aqueous species, and reactions from 1 to 5000 bars and 0° to 1000°C: Computers and Geosciences, v. 18, p. 899–947.

Jones, H.D., and Kesler, S.E., 1992, Fluid inclusion gas chemistry in east Tennessee Mississippi Valley-type districts: Evidence for immiscibility and implications for depositional mechanism: Geochimica et Cosmochimica Acta, v. 55, p. 137–154.

Kerrich, R., 1987, The stable isotope geochemistry of Au-Ag vein deposits in metamorphic rocks: Mineralogical Association of Canada Short Course Handbook, v. 13, p. 287–336.

Kyser, T.K., 1987, Equilibrium fractionation factors for stable isotopes: Mineralogical Association of Canada Short Course Handbook, v. 13, p. 1–84.

Liebenberg, L., 1968, The sulphides in the layered sequence of the Bushveld Igneous Complex: Unpublished Ph.D. thesis, Pretoria, University of Pretoria, 260 p.

Lindgren, W., 1933, Mineral deposits, 4th ed.: New York, McGraw-Hill, 930 p.

Lusk, J., Scott, S.D., and Ford, C.E., 1993, Phase relations in the Fe-Zn-S system to 5 kbars and temperatures between 325° and 150°C: ECONOMIC GEOLOGY, v. 88, p. 1880–1903.

Matsuhisa, Y., Goldsmith, J.R., and Clayton, R.N., 1979, Oxygen isotope

fractionation in the system quartz-albite-anorthite-water: Geochimica et Cosmochimica Acta, v. 43, p. 1131–1140.
Meyer, F.M., Welke, H.J., and Robb, L.J., 1986, Mineralogical and chemical characteristics of flat reefs in the Sabie-Pilgrim's Rest gold field: Geocongress '86, Johannesburg, July 7–11, 1986, Extended Abstracts p. 535–540.
Ohmoto, H., 1986, Stable isotope geochemistry of ore deposits: Reviews in Mineralogy, v. 16, p. 491–559.
Ohmoto, H., and Rye, R.O., 1979, Isotopes of sulfur and carbon, *in* Barnes, H.L., ed., Geochemistry of hydrothermal ore deposits: New York, Wiley, p. 509–567.
Ramboz, C., Pichavant, M., and Weisbrod, A., 1982, Fluid immiscibility in natural processes: Use and misuse of fluid inclusion data: II. Interpretation of fluid inclusion data in terms of immiscibility: Chemical Geology, v. 37, p. 29–48.
Redman, E., 1986, History of the Juneau gold belt: 1869–1985: U.S. Bureau of Mines Open-File Report 91–86, 78 p.
Reinecke, L., and Stein, W.G.A., 1930, Ore bodies of the Pilgrim's Rest gold field: Geological Society of South Africa Transactions, v. 32, p. 63–86.
Robb, L.J., Anhaeusser, C.R., and van Nierop, D.A., 1983, The recognition of the Nelspruit batholith north of the Barberton greenstone belt and its significance in terms of Archaean crustal evolution: Geological Society of South Africa Special Publication 9, p. 117–130.
Robert, F., and Kelly, W.C., 1987, Ore-forming fluids in Archean gold-bearing veins at the Sigma mine, Abitibi greenstone belt, Quebec, Canada: ECONOMIC GEOLOGY, v. 82, p. 1464–1482.
Roedder, E., 1984, Fluid inclusions: Reviews in Mineralogy, v. 12, 644 p.
——1990, Fluid inclusion analysis—prologue and epilogue: Geochimica et Cosmochimica Acta, v. 54, p. 495–507.
Roedder, E., and Bodnar, R.J., 1980, Geologic pressure determinations from fluid inclusion studies: Annual Reviews in Earth and Planetary Science, v. 8, p. 263–301.
Schidlowski, M., Eichmann, R., and Junge, C.E., 1975, Precambrian sedimentary carbonates: Carbon and oxygen isotope geochemistry and implications for the terrestrial oxygen budget: Precambrian Research, v. 2, p. 1–69.
Schiffries, C.M., and Rye, D.M., 1989, Stable isotopic systematics of the Bushveld Complex: I. Constraints of magmatic processes in layered intrusions: American Journal of Science, v. 289, p. 841–873.
Schiffries, C.M., and Skinner, B.J., 1987, The Bushveld hydrothermal system: Field and petrologic evidence: American Jounal of Science, v. 287, p. 566–595.
Schoonen, M.A.A., Fisher, N.S., and Wente, M., 1992, Gold sorption onto pyrite and goethite: A radiotracer study: Geochimica et Cosmochimica Acta, v. 56, p. 1801–1814.
Seward, T.M., 1973, Thio complexes of gold and the transport of gold in hydrothermal ore solutions: Geochimica et Cosmochimica Acta, v. 37, p. 370–399.
Sharp, Z.D., 1990, A laser-based microanalytical method for the in situ determination of oxygen isotope ratios in silicates and oxides: Geochimica et Cosmochimica Acta, v. 54, p. 1353–1357.
Sharpe, M.R., 1981, The chronology of magma influxes to the eastern compartment of the Bushveld Complex as exemplified by its marginal border groups: Journal of the Geological Society of London, v. 138, p. 307–326.
——1984, Petrography, classification and chronology of mafic sill intrusions beneath the eastern Bushveld Complex: South Africa Geological Survey Bulletin, v. 77, 40 p.
Sharpe, M.R., Bahat, D. and von Gruenewaldt, G., 1981, The concentric elliptical structure of feeder sites to the Bushveld Complex and possible economic implications. Geological Society of South Africa Transactions, v. 84, p. 239–244.
Shenberger, D.M., and Barnes, H.L., 1989, Solubility of gold in aqueous sulfide solutions from 150 to 350°C: Geochimica et Cosmochimica Acta, v. 53, p. 269–278.
Shieh, Y-N., and Zhang, X., 1988, Oxygen isotope geochemistry of Precambrian shales in the Kaapvaal craton, South Africa [abs.]: V.M. Goldschmidt Conference, Baltimore, MD, May 11–13, 1988, Program and Abstract, p. 74.
Sibson, R.H., Robert, F., and Poulsen, K.H., 1988, High-angle reverse faults, fluid-pressure cycling, and mesothermal gold-quartz deposits: Geology, v. 16, p. 551–555.
Smit, P.J., and Maree, B.D., 1966, Densities of South African rocks for the interpretation of gravity anomalies: South Africa Geological Survey Bulletin 48, 37 p.
Sterner, S.M., and Bodnar, R.J., 1984, Synthetic fluid inclusions in natural quartz I: Compositional types synthesized and applications to experimental petrology: Geochimica et Cosmochimica Acta, v. 48, p. 2659–2668.
Swiegers, J.U., 1949, The gold deposits of the Pilgrim's Rest gold mining district, Transvaal: Geological Society of South Africa Transactions and Proceedings, v. 51, p. 81–132.
Taylor, H.P., 1979, Oxygen and hydrogen isotope relationships in hydrothermal mineral deposits, *in* Barnes, H.L., ed., Geochemistry of hydrothermal ore deposits: New York, Wiley, p. 236–277.
Tyler, N., 1986, Oxygen- and sulphur-isotope properties of quartz and pyrite from the Pilgrim's Rest gold field, eastern Transvaal: University of the Witwatersrand, Economic Geology Research Unit Information Circular, v. 181, 4 p.
Tyler, R., 1989, Cyclic sedimentation and gold mineralization in the Malmani Dolomite Subgroup, Pilgrim's Rest-Sabie area, eastern Transvaal: Unpublished M.Sc. thesis, Johannesburg, University of the Witwatersrand, 145 p.
Van Hees, E.H., Graney, J.R., and Kesler, S.E., 1992, Fluid inclusions in native metals: II. Interpretation and implications [abs.]: PACROFI IV, 1992, p. 82.
Vennemann, T.W., and O'Neil, J.R., 1993, A simple and inexpensive method of hydrogen isotope and water analyses of minerals and rocks based on zinc reagent: Chemical Geology (Isotope Geoscience Section), v. 103, p. 227–234.
Vennemann, T.W., and Smith, H.S., 1990, The rate and temperature of reaction of ClF_3 with silicate minerals and their relevance to oxygen isotope analysis: Chemical Geology, v. 86, p. 83–88.
Walraven, F., and Hattingh, E., 1993, Geochronology of the Nebo Granite, Bushveld Complex: South African Journal of Geology, v. 96, p. 31–41.
Walraven, F., Armstrong, R.A., and Kruger, F.J., 1990, A chronological framework for the middle to late Precambrian stratigraphy of the Transvaal, South Africa: Tectonophysics, v. 171, p. 23–48.
Walsh, J.F, Kesler, S.E., Duff, D., and Cloke, P.L., 1988, Fluid inclusion geochemistry of high-grade, vein-hosted gold ore at the Pamour mine, Porcupine Camp, Ontario: ECONOMIC GEOLOGY, v. 83, p. 1347–1367.
Welhan, J.A., 1988, Origins of methane in hydrothermal systems: Chemical Geology, v. 71, p. 183–198.
Willemse, J., 1959, The "floor" of the Bushveld Igneous Complex and its relationships, with special references to the eastern Transvaal: Geological Society of South Africa Transactions, v. 62, p. 21–83.
Wybergh, W.J., 1925, The economic geology of Sabie and Pilgrims Rest: South African Geological Survey Memoirs, v. 23, 124 p.
Zietsman, A.L., 1967, The relationship between mineralisation and structure in the Pilgrim's Rest-Sabie gold-field: Unpublished Ph.D. thesis, Bloemfontein, University of the Orange Free State, 198 p.